Broadband Dielectric Resonator Antennas for WLAN Applications

Ahmed Abumazwed

A Thesis

In

The Department

of Electrical and Computer Engineering

Presented in Partial Fulfillment of the Requirements

For the Degree of Master of Applied Science at

Concordia University

Montreal, Quebec, Canada

July 2009

Your file Votre référence
ISBN: 978-0-494-63102-7
Our file Notre référence
ISBN: 978-0-494-63102-7

ABSTRACT

Broadband Dielectric Resonator Antennas for WLAN Applications

Ahmed Ali Abumazwed

Today's communications systems require use of broadband antennas to meet high capacity requirements. Furthermore, some applications require smaller antenna sizes. In this work, a broadband Dielectric Resonator Antenna (DRA) for WLAN applications is presented. The antennas presented are compact in size, have the broadside radiation patterns and high radiation efficiency. The bandwidth of the DRA depends on the dielectric material, its shape, as well as the excitation technique used to feed the antenna.

The three antennas presented in this thesis are of half cylindrical shape, mounted on ground planes and excited by aperture coupling slot. A parasitic U slot is part of the feeding network for more coupling and bandwidth enhancement. The antennas have good radiation characteristics and operate over a wide band of frequencies. Ansoft HFSS is used for the antenna simulation. CST Microwave studio is also used to compare the accuracy of time domain and frequency domain analysis of the DRAs. The DR material is Rogers RO3010 ™ with $\varepsilon_r = 10.2$, and a dielectric loss tangent of 0.0035. The substrate material is Rogers RT/Duroid 5880 ™ with $\varepsilon_s = 2.2$, a loss tangent of 0.0009, and 0.767 mm thickness.

The half-cylindrical DRA is used to have the $TE_{01\delta}$ mode excited. The radiation patterns of the three antennas are similar to that of a magnetic monopole which has the broadside radiation pattern. Parasitic U-shaped slots are used with the three presented antennas to enhance the bandwidth by exciting a dual resonant frequency in the $TE_{01\delta}$ mode. These slots have similar radiation characteristics to those of the half cylindrical DRAs so the overall radiation patterns of these antennas are not deteriorated.

For the fabricated antennas, they have broadside radiation characteristics in H and E planes. As for the impedance bandwidth, the half cylindrical DRA has 24 % fractional bandwidth. For the half cylindrical DRA backed with a rectangular dielectric resonator, 32% bandwidth is achieved. A bandwidth of 29% is achieved in the case of half volume Elliptical DRA. The gain of the three antennas slightly changes around 5 dBi which is good for the WLAN applications.

ACKNOWLEDGEMENTS

It is my profound pleasure to thank all of those who helped me out to finish my M.Sc. thesis.

I would like to highly appreciate the Libyan Government and The Higher Institute of Electronics, Bani Walid, Libya for their financial support. Many thanks must go to Concordia University for the academic support.

I would like to express my gratitude to Prof. Abdel Razik Sebak whose support, encouragement, and stimulating suggestions helped me in all the time during the preparation for this thesis.

Many thanks must go to my colleagues in the department for their help with using Lab view during the measurements. I would also like to thank Mr. Jules Goutier, in École Polytechnique de Montréal, for the technical help and his continuous advices during the antenna fabrication process.

Last but not least, I would like to thank my family especially my mother who always supports and prays for me. I would like to thank my wife for the sacrifices she has made to support me in undertaking my master studies.

Ahmed Abumazwed

DEDICATION

This thesis is dedicated to my father's soul. It is also dedicated to my mother, who taught me the patience and the perseverance.

TABLE OF CONTENTS

Chapter Three

Chapter Four

List of Figures

Figure

Abbreviations

AP	Access Point
BPSK	Binary Phase Shift Keying
CST-MWS	Computer Simulation Technology-Microwave Studio
DR	Dielectric Resonator
DRA	Dielectric Resonator Antenna
EDRA	Elliptical Dielectric Resonator Antenna
FDTM	Finite Difference Time Domain
FEM	Finite Element Method
FIT	Finite Integration Technique
HE	Hybrid Magnetic-Electric
HFSS	High Frequency Structure Simulator
MoM	Method of Moments
OFDM	Orthogonal Frequency Division Multiplexing
PBA	Perfect Boundary Approximation
QAM	Quadrture Amplitude Modulation
Q-factor	Quality factor
QPSK	Quadrture Phase Shift Keying
RDR	Rectangular Dielectric Resonator
TE	Transverse Electric
TLM	Transmission Line Method
TM	Transverse Magnetic
WLAN	Wireless Local Area Network

List of Symbols

δ	Fraction of the half wavelength
ΔL_f	Stub length
ε_{eff}	Effective permittivity of a DRA
ε_r	Dielectric Constant
ε_s	Substrate dielectric constant
φ	Azimuth direction
λ_0	Free space resonant frequency
λ_g	Wavelength in a DRA
θ	Elevation direction
a	Radius of cylindrical or spherical DRA
E	Electrical field intensity
f_x	Resonant frequency for the $TE^x_{\delta 11}$
f_y	Resonant frequency for the $TE^y_{1\delta 1}$
f_z	Resonant frequency for the $TE^z_{11\delta}$
H	Magnetic field intensity
h	DRA height
H_{total}	Total height of a DRA
k_0	Wave number in free space
k_x	Wave number in x direction

k_y	Wave number in y direction
k_z	Wave number in z direction
L	DRA length
L_f	Microstrip length
L_s	Inner slot Length
L_{s1}	Length of the horizontal arm of the U slot
L_{s2}	Length of the parallel arms of the U slot
$\hat{n}$	A normal to the DR surface
p	Shift of the DRA center from the ground plane center
r	Radial direction
R_1/R_2	Minor to Major Axis of the Half EDRA
t	Substrate thickness
W	DRA width
W_f	Microstrip Line width
w_s	Inner slot width
w_{s1}	Width of the horizontal arm of the U slot
w_{s2}	Width of the parallel arms of the U slot
Z_0	Characteristic impedance of the microstrip line

Chapter One

Introduction

This chapter presents the objective of this thesis and motivation to fulfill these objectives. A brief history of dielectric resonator antenna (DRA) is then given. Major characteristics of DRAs and comparison with other conventional antennas are discussed.

1.1 Problem Statement and Motivation

In today's communications systems, it is desirable to have high efficiency wireless systems with wide bandwidth and small equipment size. There are many WLAN standards employing the 2.4 GHz and 5 GHz bands. The IEEE.802.11 standard has many versions using these bands. Table 1.1 compares these standards.

WLAN used in this thesis is based on the IEEE.208.11a standard in the 5 GHz band using the Orthogonal Frequency Division Multiplexing (OFDM) offering 12 channels without overlapping which allows 12 Access Points (AP) operating in the same vicinity. The OFDM uses 52 subcarriers that are modulated using BPSK, QPSK, 16 QAM, or 64 QAM depending on the desired speed [1]. A system with such specifications requires a high efficient broadband antenna. Moreover, In today's technology, it is required to have small size wireless devices which requires smaller antennas.

	IEEE.208.11.a	IEEE.208.11.b	IEEE.208.11.g
Frequency Band (GHz)	5.15-5.25 5.25-5.35 5.725-5.825	2.4-2.4835	2.4-2.4835 5.25-5.35
Modulation technology	OFDM	DSSS/CCK	OFDM, PBCC
Max. Data Rate	54 Mbps	2 Mbps	54 Mbps
Range coverage	<100 m	<50 m	<50 m
Interference with other devices	Less	Significant	Significant

Table 1.1: Comparison of the IEEE.208.11 standards.

Different recent efforts are made to design antennas which can operate effectively for the recent wireless applications. To meet the high capacity requirements for wireless systems, it is desirable for these antennas to operate as broadband antennas. As for the small wireless devices, the antenna has to be compact and easily embedded to such small devices. Compact dielectric resonator antennas have been proposed to be embedded in the small sized wireless devices. However, minimizing the antenna size may affect other antenna parameters such as the antenna radiation patterns and operating bandwidth. On the other hand, much research have been conducted to design wideband DRAs and develop techniques to improve their bandwidth. Some of these techniques are complicated and difficult to implement and others increase the overall size of the DR

antenna. Therefore, there is a trade off between the antenna size and the operating bandwidth and the radiation patterns.

In this thesis, some techniques are introduced to design compact DRAs. Using a half volume DRA with certain resonant modes being excited in the modified shape makes it an efficient radiator with less size. A compact Half- Elliptical DRA is also presented which offers more degree of design flexibility to facilitate the design of a compact DRA. As for the bandwidth enhancement, there are many techniques used with the DRA and other types of antennas and the feeding mechanism is one of the easiest used techniques. This thesis proposes a feeding network of the DRA composed of a rectangular slot surrounded by a parasitic U-shaped slot. The rectangular slot is used as the main coupling element whereas the U-shaped slot is used as a supporting coupling element and for the bandwidth enhancement.

1.2 Introduction to DRAs

Dielectric Resonator Antenna (DRA) was first proposed by Long et al. [2] in 1983. It has been found that using microstrip patch antennas at higher frequencies was inefficient due to their high ohmic losses at such a frequency band. Cylindrical Dielectric Resonators (DRs) were used as energy storage devices but many difficulties, due to the leakage, have been reported for such kind of storage devices. The leaky nature of the cylindrical DRs storage devices has been considered as an advantage to use them as radiating elements. The radiated fields are due to the lower order modes being excited in

the DRs. Since then, many investigations have been reported about the DRAs with different shapes and their characteristics have been examined [2]-[4]. It has been reported that DRAs have many advantages including high efficiency, light weight, and diversity of feeding techniques used to excite the antenna which makes this kind of antennas a good candidate for many applications.

After DRs proved themselves as good radiating elements candidates, much research have been concentrated on improving the characteristics of such kind of antennas. Many feeding techniques have been examined to excite the DRAs to realize the different feeding schemes of the DRAs. The bandwidth enhancement techniques have been going on to satisfy the requirements of the new wireless technology [5-15].

Many efforts have also directed towards DR antenna arrays. A linear DRA array has been first introduced by Birand and Gelsthorpe in the early 1980's [3]. The first study of a planar array was introduced by Haneishi and Takazawa [4] . In the mid-1990's, more research have been devoted to the DRA array with steering beam capabilities. Moreover, when the DRA is made of a high permittivity with slight dissipation losses , it can handle high power. The high power capability is considered as an advantage when used in radar applications [16].

1.3 Characteristics of Dielectric Resonator Antennas (DRAs)

The DRA size depends mainly on the substrate material used for the design. It is proportional to $\frac{\lambda_0}{\sqrt{\varepsilon_r}}$ where λ_0 is the wavelength at the resonant frequency in free space, and ε_r is the relative permittivity of the used substrate material.

The DRA size also depends on the type of the DR used as a radiating element. If the DRA is made of a high permittivity dielectric material, this would lead to a smaller DRA antenna. Accordingly, the quality factor will increase and the bandwidth will decrease. Moreover, the size of the radiating DR for a specified dielectric material also affects the Q- factor of the antenna. The DR geometry also affects the resonant frequencies as the DRA could be formed to many geometries.

DRAs has many advantages over conventional radiating elements. Although the microstrip antennas have the small size, light weight characteristics, the presence of surface waves and conductor losses especially at high frequency bands deteriorate the radiation efficiency. DRAs offer high radiation efficiency even if they are used in high frequencies applications. This is because of the low ohmic losses and there is no surface waves when using such kind of antennas.

DRAs may be used at a wide range of frequencies starting from 1.3 GHz up to 40 GHz. As well there is a wide range of dielectric materials with different relative

permittivity values which could be used starting from 8 up to 100 which offers a design flexibility to control the antenna size and/or the bandwidth .

Another advantage of the DRAs is that they could be excited by many feeding mechanisms. They can be fed by probes, aperture slots, coplanar waveguides, microstrip lines, and waveguides for potential integration with many technologies including the chip technology.

From a shape point of view, the antenna may be formed in cylindrical, rectangular, spherical, or by deformation of these shapes. This gives more flexibility to the antenna design. Many modes could be excited within the DRA depending on the DR geometry and the feeding mechanism involved to excite the antenna. Some of these modes have omnidirectional or broadside radiation patterns which, of course, could be involved in many antenna applications. Moreover, a DRA with certain modes of radiation could be combined with another antenna having the same modes to offer a wideband hybrid DRA antenna [17][18].

For the DRA array, there is no mutual coupling between the elements due to the surface waves. The mutual coupling in a DRA array is due to the space waves [6]. Since the surface waves are not supported by DRAs, the scan blind problems with large microstrip arrays can be solved. The scan blind is the signal loss due to the mutual coupling and it occurs when the main beam is steered to the low elevation angles in microstrip array [16].

1.4 Organization of thesis

Chapter 2 reviews DRA geometries with more details about the half cylindrical and rectangular DRA modes of operation and the feeding mechanisms especially the aperture slot feeding technique because they are used in this thesis. Review of bandwidth enhancement techniques are also given. Numerical techniques used to analyze DRAs are highlighted in chapter 2.

In Chapters 3, DRA design formulae are given as the procedure of the DRA design is explained in detail. These equations are considered as a starting point and the antennas' dimensions should be optimized by using software packages. Ansoft HFSS [19] and CST microwave studio [20] are used to optimize the antennas in this work. An introduction to these software packages is given in chapter 3 as the principle of numerical technique used in each package is highlighted.

Chapter 4 is devoted for a parametric study and all related results for the three optimized antennas; the half-cylindrical DRA, the modified half-cylindrical DRA, and the elliptical half-cylindrical compact DRA. The optimized antennas have been fabricated and experimentally tested, all the experimental results will be included in chapter 4. For all antennas, design formulae are used first, then a parametric study is carried out to improve the antenna characteristics, Ansoft HFSS 10 [19] and CST microwave studio [20] are used for this purpose. Chapter 5 concludes the work done in this thesis and some recommendations are also proposed for a better antenna performance.

Chapter 2

Literature review and Dielectric Resonator Antenna Parameters

2.1 Introduction

In this chapter, the dielectric resonator antenna is briefly explained. A general review on DRAs is presented including DRA modes of propagation, geometries, feeding mechanisms, and some bandwidth enhancement techniques.

2.2 General Description of DRAs

A DRA is a high radiation efficiency radiator. As its name implies, a dielectric resonator is used to be operating as the radiating part. Some people may think that the dielectric resonators are only used with filters. This is because of the high Q-factor which the DRs have at the high order modes. If a dielectric resonator is excited for the lower modes, it will have a low Q-factor and can operate as an antenna with good characteristics. The DRs can be formed in different shapes offering more design flexibility, it can be rectangular, cylindrical, hemispherical, or their deformations. The shapes of DRAs are discussed in more details in section 2.4. These different DRAs can be fed by various coupling mechanisms exciting many radiating modes with different radiation characteristics. In general, DRAs can be designed to be placed on ground plane

or on a lower permittivity substrate. Figure 2.1 demonstrates a DRA on ground plane, and fed by a microstrip line.

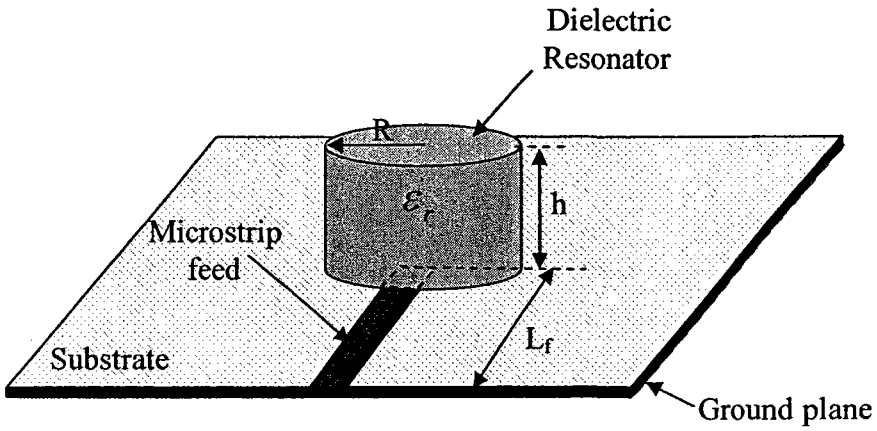

Figure 2.1: A sketch of a DR Antenna.

2.3 DRA Resonant Modes

This section describes the modes within the arbitrary DRA geometry. However, the modes for each DRA geometry will be presented in more detail in the following sections. The modes being excited in a DRA of an arbitrary shape can be classified as confined and non-confined modes [21]. Both modes satisfy the following condition

$$\vec{E} \cdot \hat{n} = 0 \qquad (2.1)$$

Where $\vec{E}$ is the electric field intensity, and $\hat{n}$ is the normal to the DRA surface. As mentioned above, both the confined and non-confined modes satisfy equation 2.1 which

is a condition of a magnetic wall. Another condition of a perfectly magnetic wall is satisfied by the confined modes is

$$\hat{n} \times \vec{H} = 0 \qquad (2.2)$$

Where $\vec{H}$ is the magnetic field intensity. This equation is not satisfied by the non-confined modes. The lower order confined modes radiate like electric dipoles whereas the lower non-confined modes radiate like magnetic dipoles [21]. Moreover, It has also been shown that the confined modes are only supported by dielectric bodies of revolution such as spherical and cylindrical DRAs [22]. Accordingly, rectangular DRA supports the non-confined modes only. More detailed explanation to each category of the modes will be presented in the following sections.

2.4 DRA shapes

The cylindrical geometry was the first proposed shape for the DR antenna in the early 1980's. Later, the rectangular DRA was introduced to add more design flexibility. The hemispherical DRA has also attracted some researchers and the results were satisfactory for this geometry as well. This section is devoted for the basic DRA geometries, their characteristics, and the modes excited within these DRAs.

2.4.1 Rectangular DRA

Due to the high degree of design flexibility, rectangular DRAs have attracted many researchers to achieve the desirable antenna characteristics in different

applications. The rectangular DRA is characterized by a length L, a width w, a height h, and a dielectric constant of the material used for the DRA (ε_r). Figure 2.2 shows the rectangular DRA geometry. The w/L, and h/L aspect ratios offer an independent design flexibility. As for the Q-factor, it is strongly affected by the dielectric constant of the Dielectric resonator being used for the design. The two aspect ratios (w/h, L/h) also affect the Q-factor.

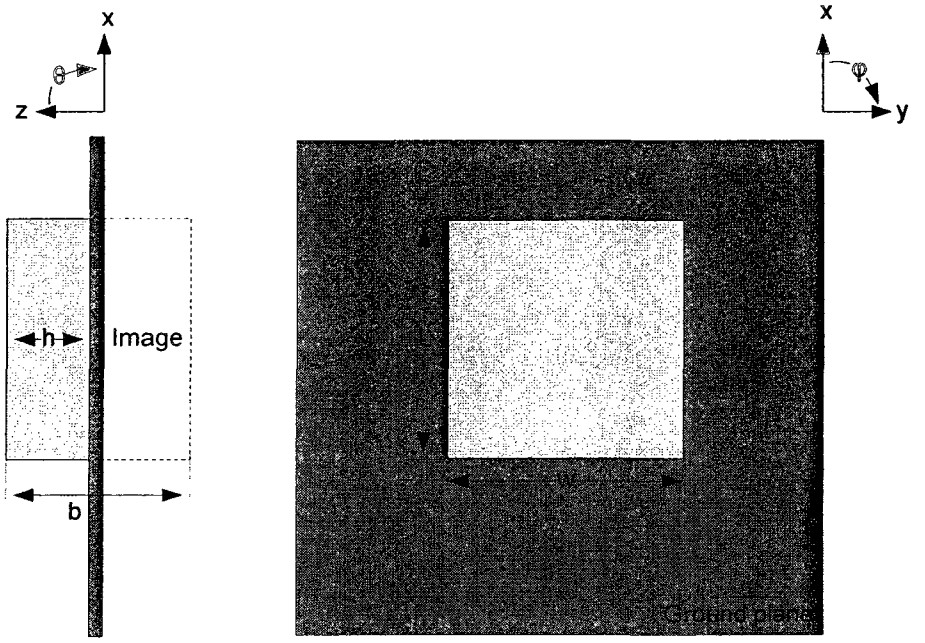

Figure 1.2: Rectangular DRA geometry

The rectangular DRA supports the TE modes in the x, y, or z directions which radiate like short magnetic dipoles in these directions [21]. The resonant frequency of each mode depends on the size of the rectangular DR. as the larger side of the rectangle corresponds to a smaller resonant frequency at the direction of the side orientation.

The rectangular DRA has three dimensions in x, y, and z directions as shown in Figure 2.2. The fields of the lower order modes are $TE^{x}_{\delta 11}$, $TE^{y}_{1\delta 1}$, and $TE^{z}_{11\delta}$ [23][24]. If the rectangular DRA has the dimensions w>L>h, the resonant frequencies for the three TE modes in x, y, and z directions are $f_x < f_y < f_z$. The modes have similar analysis, so the $TE^{x}_{\delta 11}$ is carried out here. Using the Waveguide Cavity model, the field components could be derived from the z directed magnetic potential in the x direction [21]. This gives

$$H_x = \frac{\left(k_y^2 + k_z^2\right)}{j\omega\mu_0}\cos(k_x x)\cos(k_y y)\cos(k_z z) \tag{2.3}$$

$$H_y = \frac{\left(k_y k_x\right)}{j\omega\mu_0}\sin(k_x x)\sin(k_y y)\cos(k_z z) \tag{2.4}$$

$$H_z = \frac{\left(k_z k_x\right)}{j\omega\mu_0}\sin(k_x x)\cos(k_y y)\sin(k_z z) \tag{2.5}$$

$$E_x = 0 \tag{2.6}$$

$$E_y = k_z \cos(k_x x)\cos(k_y y)\sin(k_z z) \tag{2.7}$$

$$E_z = -k_y \cos(k_x x)\sin(k_y y)\cos(k_z z) \tag{2.8}$$

where $k_x \tan(k_x d/2) = \sqrt{(\varepsilon_r - 1)k_0^2 - k_x^2}$ (2.9)

and $k_x^2 + k_y^2 + k_z^2 = \varepsilon_r k_0^2$ (2.10)

The $e^{j\omega t}$ term is removed from the equations for the simplicity. Applying the magnetic wall boundary condition $\vec{E} \cdot \hat{n} = 0$ at the air-dielectric interfaces parallel to z axis, the wave numbers are obtained

$$k_y = \frac{m\pi}{w} \text{ and } k_z = \frac{n\pi}{b}, \text{ m, n are positive integers.}$$

δ is the fraction of a half-cycle of the field variation along the z direction and equals

$$\delta = \frac{k_x}{\pi / L} \tag{2.11}$$

The lower order mode (m=n=1) fields are sketched in Figure 2.3.

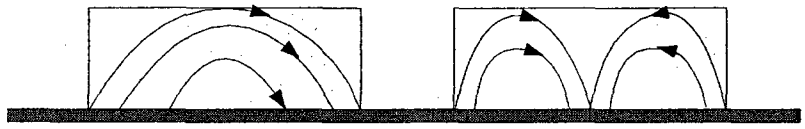

Figure 2.3: Modes in rectangular DRA (a) $TE^x_{\delta 11}$, (b) $TE^x_{\delta 21}$

2.4.2 Hemispherical DRA

The hemispherical DRA placed on ground plane is shown in Figure 2.4. The hemispherical DRA has less degree of design flexibility than the rectangular DRA as it consists of a radius a around the center of the sphere. The size of the DRA depends on the dielectric constant of the spherical DR as well as the resonant frequency.

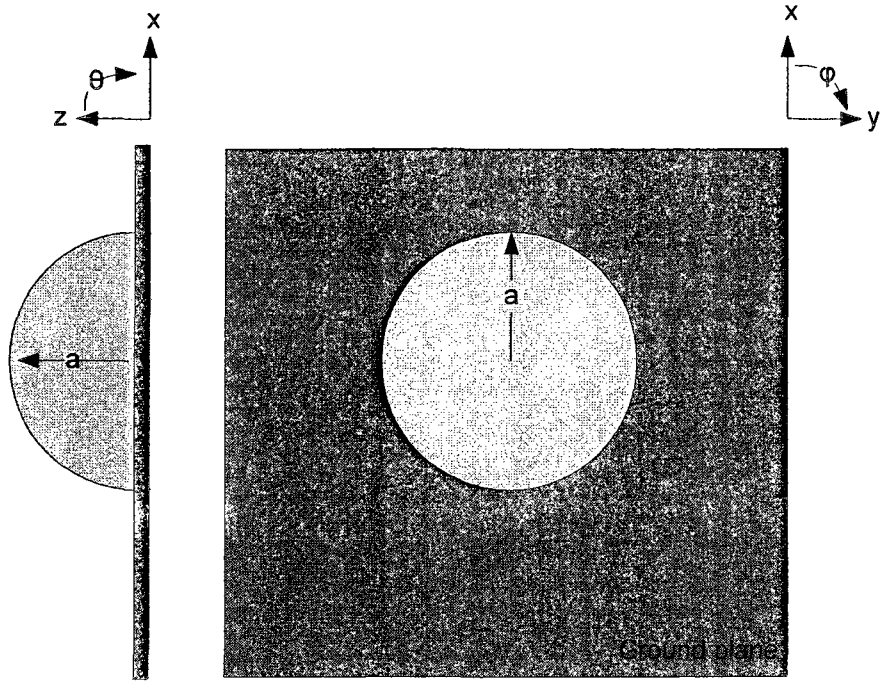

Figure 2.4: Hemispherical DRA

The modes in this DRA are divided into Transverse Electric (TE) where the radial component of the electric field (E_r) is zero, and Transverse magnetic (TM) as the radial component of the magnetic field (H_r) is zero. The TE_{111}, and TM_{101} modes are the two modes of interest in hemispherical DRA. The subscripts refer to the field variation in the radial (r), azimuth (φ), and elevation (θ) directions in the spherical coordinate system. The TE_{111} mode radiate like a short horizontal magnetic dipole, whereas the TM_{101} mode radiates like a short electric monopole. The field patterns of this DRA at the TE_{111} and TM_{101} modes are shown in Figure 2.5. As this kind of geometries is out of the scope of this thesis, no details about the field equations will be presented. The equations of the fields inside the resonator and the plots of these fields can be found in [25][26].

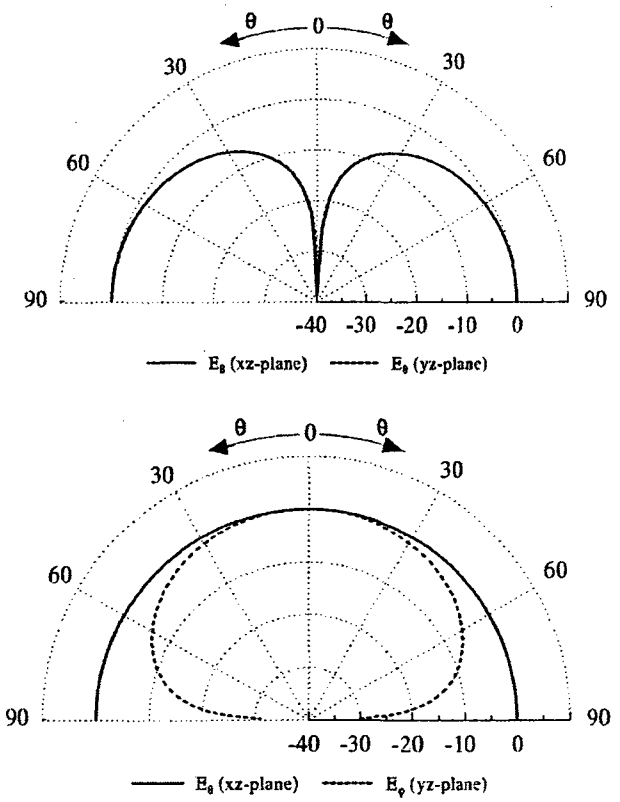

Figure 2.5: Radiation patterns of a hemispherical DRA on ground plane for (a) TE_{111}, (b) TM_{101} modes. [27], pp.148-149.

2.4.3 Cylindrical DRA

The cylindrical DRA having a height (h) and a radius (a) is shown in Figure 2.6. The (a/h) aspect ratio offers more degree of design flexibility than the hemispherical DRA. This ratio also determines the quality factor and the resonant frequency. For example, a DRA with a large height (h) and a small radius (a) could be designed to resonate at the same frequency of another DRA with less height (h) and larger radius (a). However, the two antennas will have different Q-factor affecting the DRA bandwidth.

Consequently, the cylindrical DRA could offer two Q-factors for a given resonant frequency.

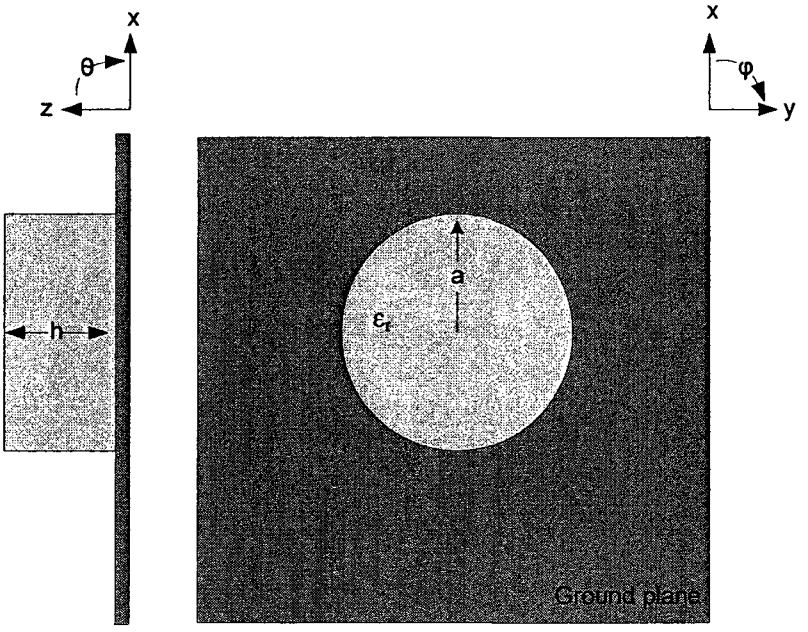

Figure 2.6: Cylindrical DRA Geometry.

As for the modes of radiation in the cylindrical DRA. There are three modes; TE, TM, and hybrid modes (HE if E_z component is dominant, or EH if H_z component is dominant). The $TE_{01\delta}$, $TM_{01\delta}$, and $HE_{11\delta}$ modes are mostly used for the DRA applications. The subscripts refers to the field variations in the azimuth (φ), radial (r), and axial (z) directions in the cylindrical coordinate system. The $0 \leq \delta \leq 1$ as it approaches one for the high permittivity DR.

To derive the fields for the cylindrical DRAs, a magnetic wall (perfect open circuit) condition is assumed for the z-component of the magnetic field (H_z) is zero at all surfaces along the z axis and the tangential components of the electric and magnetic fields are

continues across the surfaces parallel to z axis. For a cylindrical DRA operating in the $TE_{01\delta}$ mode are approximated by [28][29]:

$$H_z \alpha\ J_0(\beta r)\cos\left(\frac{\pi}{2h}z\right) \tag{2.12}$$

$$H_r \alpha\ J_1(\beta r)\sin\left(\frac{\pi}{2h}z\right) \tag{2.13}$$

$$E_\phi \alpha\ J_1(\beta r)\cos\left(\frac{\pi}{2h}z\right) \tag{2.14}$$

$$E_z = E_r = H_\phi = 0 \tag{2.15}$$

$J_0(\beta r)$ and $J_1(\beta r)$ are Bessel functions of the first kind. β is the solution to $J_0(\beta a) = 0$. The fields for the $TM_{01\delta}$ mode are similar and could be obtained by interchanging the electric and magnetic fields components. The $TE_{01\delta}$ radiates like a short magnetic monopole whereas the $TM_{01\delta}$ radiates like a short electric monopole similarly to the TM_{101} mode in the hemispherical DRA case. See Figure 2.7.

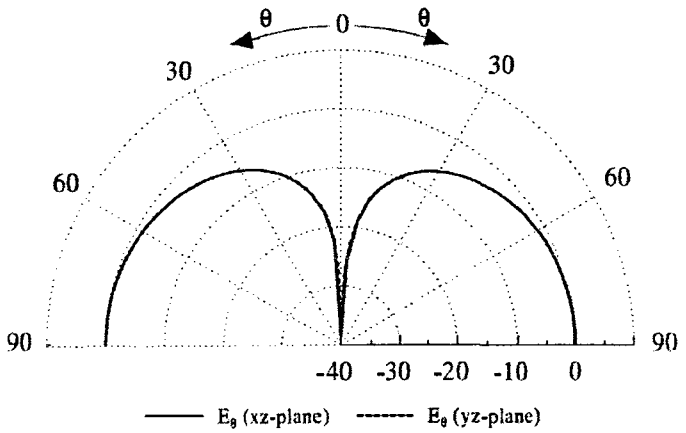

Figure 2.7: Radiation patterns of a cylindrical DRA operating in the $TM_{01\delta}$ mode. [27]

As for the $HE_{11\delta}$, the field components are expressed as:

$$E_z \propto J_1(\alpha r)\cos\left(\frac{\pi}{2h}z\right)\begin{cases}\cos\phi\\ \sin\phi\end{cases} \tag{2.16}$$

$$E_r \propto \frac{\partial J_1(\alpha r)}{\partial(\alpha r)}\sin\left(\frac{\pi}{2h}z\right)\begin{cases}\cos\phi\\ \sin\phi\end{cases} \tag{2.17}$$

$$E_\phi \propto J_1(\alpha r)\sin\left(\frac{\pi}{2h}z\right)\begin{cases}\sin\phi\\ \cos\phi\end{cases} \tag{2.18}$$

$$H_r \propto J_1(\alpha r)\cos\left(\frac{\pi}{2h}z\right)\begin{cases}\sin\phi\\ \cos\phi\end{cases} \tag{2.19}$$

$$H_\phi \propto \frac{\partial J_1(\alpha r)}{\partial(\alpha r)}\cos\left(\frac{\pi}{2h}z\right)\begin{cases}\cos\phi\\ \sin\phi\end{cases} \tag{2.20}$$

$$H_z \approx 0 \tag{2.21}$$

where α is the solution to $J_1(\alpha a)=0$. In the above equations, $\sin(\phi)$ or $\cos(\phi)$ is chosen according to the feed location [27]. The $HE_{11\delta}$ mode radiates like a short horizontal magnetic dipole similar to the TE_{111} mode in the hemispherical DRA. [27]

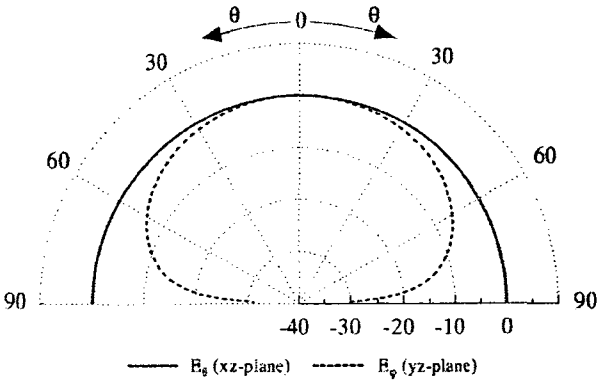

Figure 2.8: Radiation patterns of a cylindrical DRA operating in the $HE_{11\delta}$ mode. [27]

2.4.4 Half-Cylindrical DRA

Half-cylindrical DRAs are used to offer a compact DRA as image theory applies in this case. For the half-cylindrical DRA shown in Figure 2.9, the field radiation patterns for the $TE_{01\delta}$ and $HE_{12\delta}$ modes are shown in Figure 2.10. The $TE_{01\delta}$ mode radiates like a short horizontal magnetic dipole similarly as the radiation pattern of the $HE_{11\delta}$ in the cylindrical DRA and the TE_{111} mode in hemispherical DRA. As for the $HE_{12\delta}$ mode, it radiates like a short electric monopole as the radiation patterns of the $TM_{01\delta}$ and TM_{101} in the cylindrical and the hemispherical DRAs respectively.

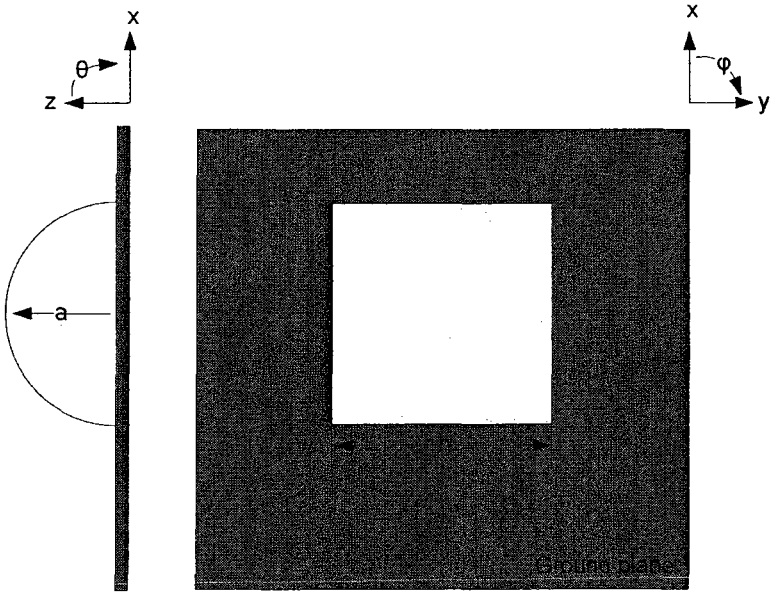

Figure 2.9: Cylindrical DRA Geometry.

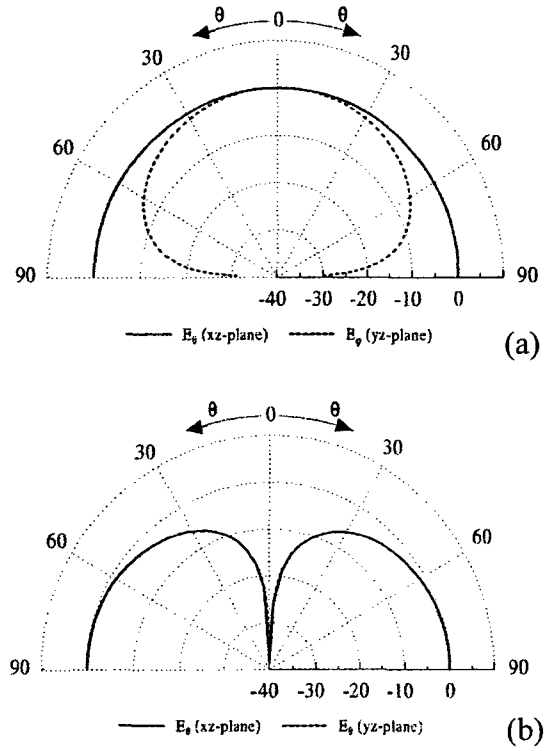

Figure 2.10: Radiation patterns of a half-cylindrical DRA on ground plane for (a) $TE_{01\delta}$, (b) $HE_{12\delta}$.[27],pp.148-149.

2.5 Coupling Mechanisms

This section highlights several feeding schemes mostly used for DRA excitation. The DRA can be excited by probes [2][30-32], aperture coupling with microstrip feed line [33-38], aperture coupling with coaxial feed [39][40], direct microsrip feed [41][42], and coplanar feed line [43]. The modes being excited in a DRA are dependant on the feeding scheme used to excite the DRA and accordingly the radiation patterns of that DRA could be easily known.

2.5.1 Probe Coupling

Coaxial feed line is used to excite the DRA especially for low frequency where the aperture coupling is large to be realized. A rectangular DRA fed by a probe is shown in figure 2.11. The advantage of probe coupling is that there is no need for a matching network to a 50 ohm system.

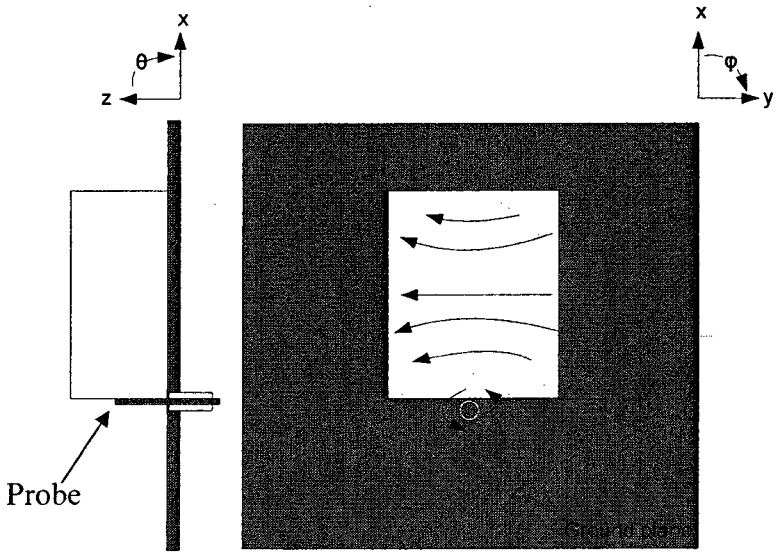

Figure 2.11: Rectangular DRA fed by a probe exciting the $TE_{\delta 11}$.

If the probe is located adjacent to the DRA, the $TE_{\delta 11}$ mode will be excited in a rectangular DRA , the $HE_{11\delta}$ and the $TE_{01\delta}$ will be excited in the cylindrical and half-cylindrical DRA respectively as shown in Figure 2.12 . To excite the $TM_{01\delta}$ mode in the cylindrical or ring DRAs, the probe must be in the centre of the DRA as shown in Figure 2.12 (c). This requires drilling into the DRA which is practically undesirable.

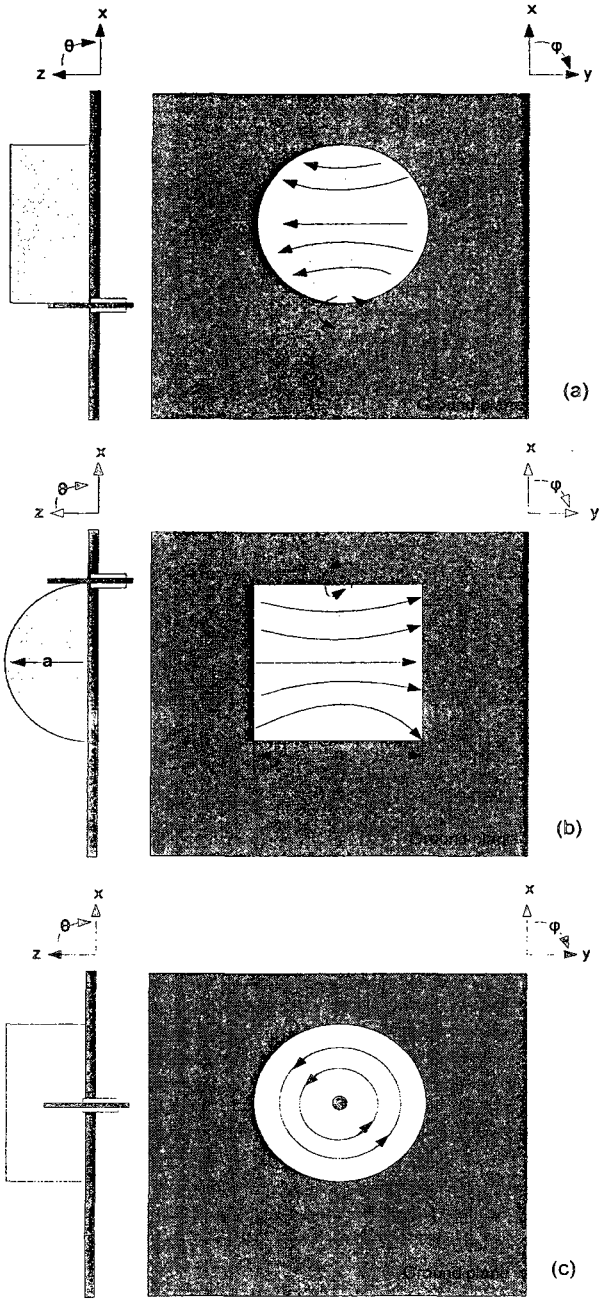

Figure 2.12: Probe Excitation. (a) $HE_{11\delta}$ mode in a cylindrical DRA, (b) $TE_{01\delta}$ mode in a half-cylindrical DRA, and (c) $TM_{01\delta}$ mode in a cylindrical DRA.

2.5.2 Microstrip Line coupling

There are several technique used to implement the microstrip line coupling to DRAs depending on the location of the microstrip with respect to the DRA to be excited. The microstrip line could be extended underneath the DRA by a space (ΔL_f) for a direct coupling , or adjacent to the DRA by a space (s). The coupling strength could be controlled by adjusted by ΔL_f and s. These two techniques are shown in Figure 2.13 [44]. The $TE^{x}_{\delta 11}$ and $HE_{11\delta}$ modes could be excited by the microstrip line feeding technique in the rectangular and cylindrical DRAs respectively. This is shown in Figure 2.14 .

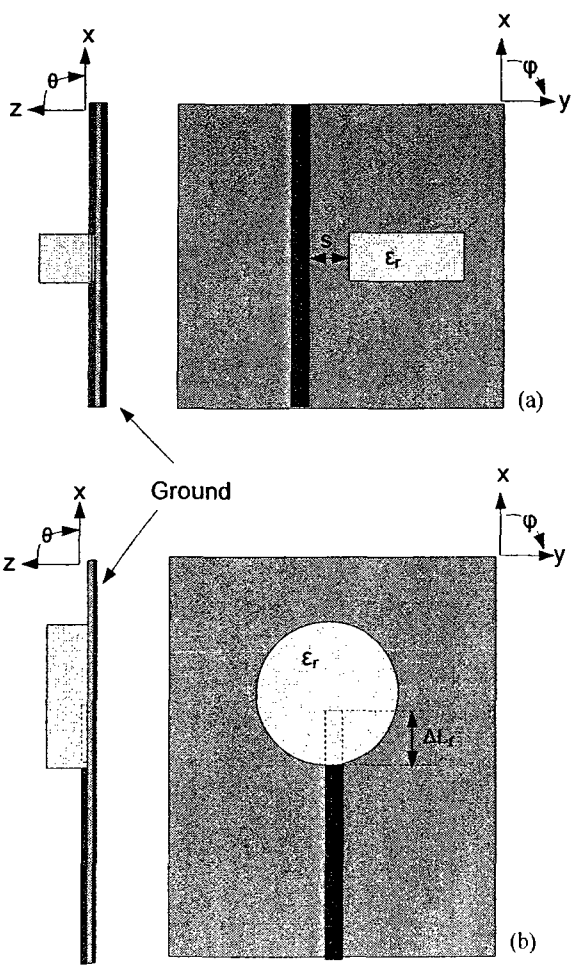

Figure 2.13: Microstrip coupling, (a) proximity coupling, (b) Direct coupling.

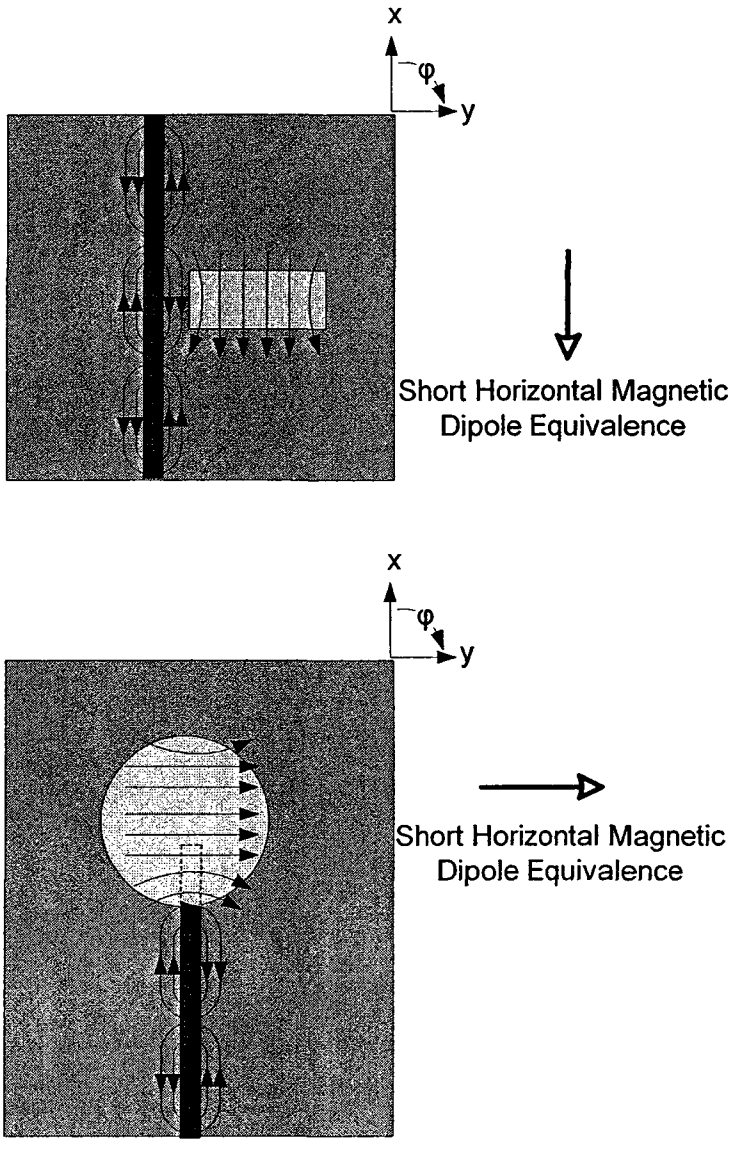

Figure 2.14: Magnetic fields and equivalent radiation models of microstrip coupling.

2.5.3 Coplanar coupling

Another interesting coupling technique is the coplanar coupling. In this techniques, The DRA can be fed directly by the short circuit coplanar feed. The coplanar

stub loaded lines or coplanar loops are used for controlling the impedance matching of the DRA. Theses coupling techniques are shown in Figure 2.15 [45][46]. The coupling strength depends on the location of the DRA from the coplanar used for the excitation. $HE_{11\delta}$ and $TE_{01\delta}$ modes could be excited in a cylindrical DRA by moving a coplanar loop from an edge of the DRA to its center. The coplanar dimensions should be chosen carefully as they should be large enough for more coupling but small enough to avoid a large back lobe level.

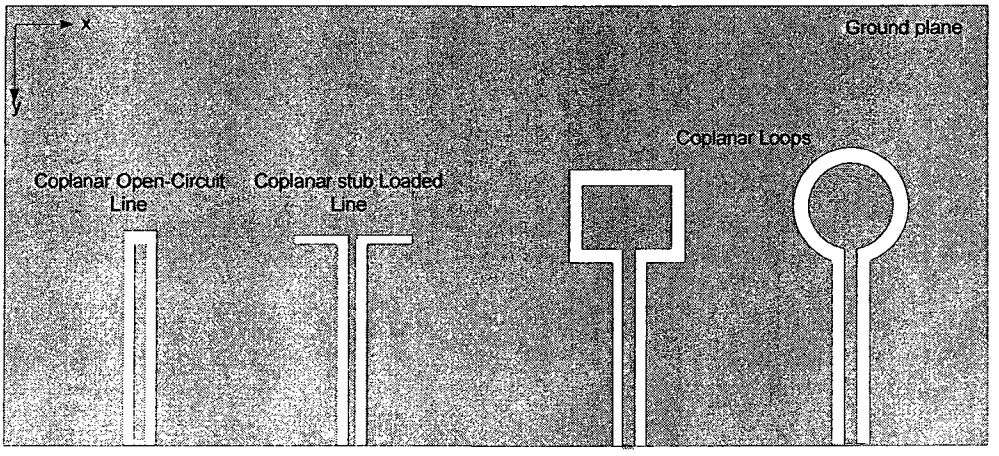

Figure 2.15: Different Coplanar feeding techniques.

2.5.4 Aperture coupling

Aperture coupling is a technique where the feed line is located below the ground plane which offers the advantage of minimizing the spurious radiations and the unwanted coupling from the feed line. Apertures may be rectangular, annular, cross-shaped, or C-shaped. Figure 2.16 shows these aperture coupling techniques.

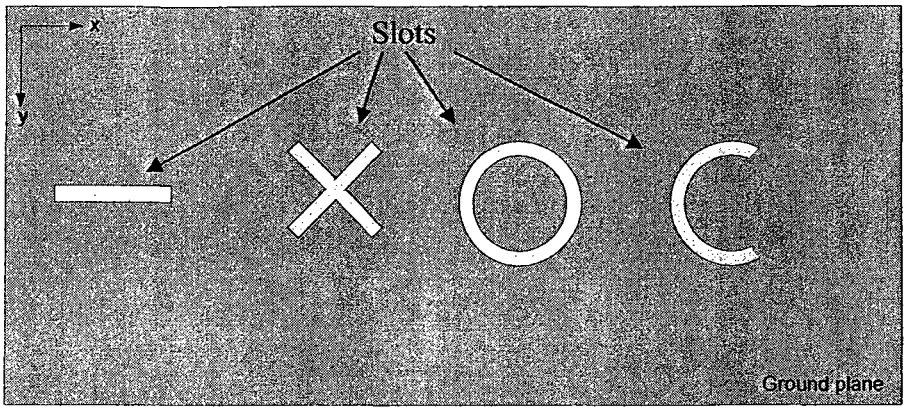

Figure 2.16 Aperture slot coupling with various shapes.

The small rectangular slot is most widely used to feed DRAs [47-51]. The slot should be electrically small to suppress the back lobe levels. The annular aperture coupling has been used to feed cylindrical DRAs [50]. The C-shaped apertures and the cross-shaped apertures have been used for the circular polarization applications [52][53]. Aperture coupling could excite the $TE^{x}_{\delta 11}$ mode in rectangular DRAs [51] as shown in Figure 2.17. For more impedance matching, the DRA should be offset to ensure a strong coupling to the internal magnetic fields.

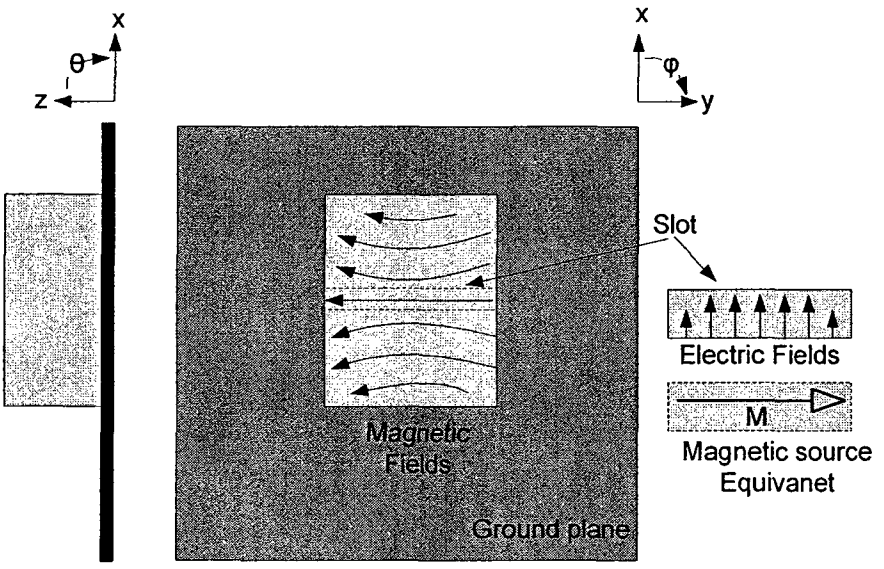

Figure 2.17 Fields in aperture slot coupled rectangular DRA.

The rectangular slot has also been used to excite the $HE_{11\delta}$ mode in cylindrical DRAs [54] and the $TE_{01\delta}$ mode in half-cylindrical DRAs [47] as shown in Figure 2.18.

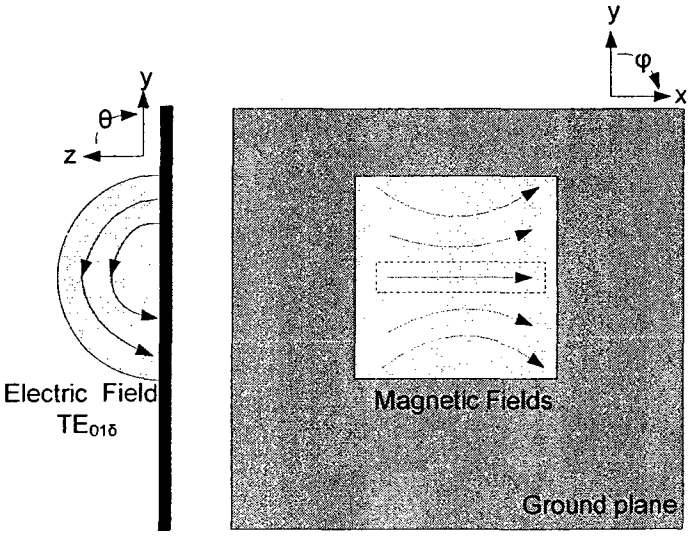

Figure 2.18 Fields in cylindrical and half-cylindrical DRA.

2.6 Bandwidth Enhancement techniques

This sections highlights several approaches used to improve the bandwidth of the DRAs. The bandwidth could be improved by adjusting the feeding mechanism, using multiple DRAs, orienting the geometry of the DRA, or using hybrid DRAs. These techniques are explained in some detail in the following subsections.

2.6.1 Excitation method

The excitation techniques have been discussed earlier. The most widely used techniques are the aperture slot, the direct microstrip feed, and the probe feeding. For the rectangular slot, the bandwidth could be improved by extending the slot underneath the DRA so they will operate as radiating slots as shown in Figure 2.19 [6]. In this case, the radiating part of the slot enhances the impedance bandwidth but on the expense of the radiation pattern of the DRA as the back lobe level of this antenna is high which might be caused by the spillover due to the small ground plane. If a larger ground plane is used, this problem could be solved but on the expense of the antenna size.

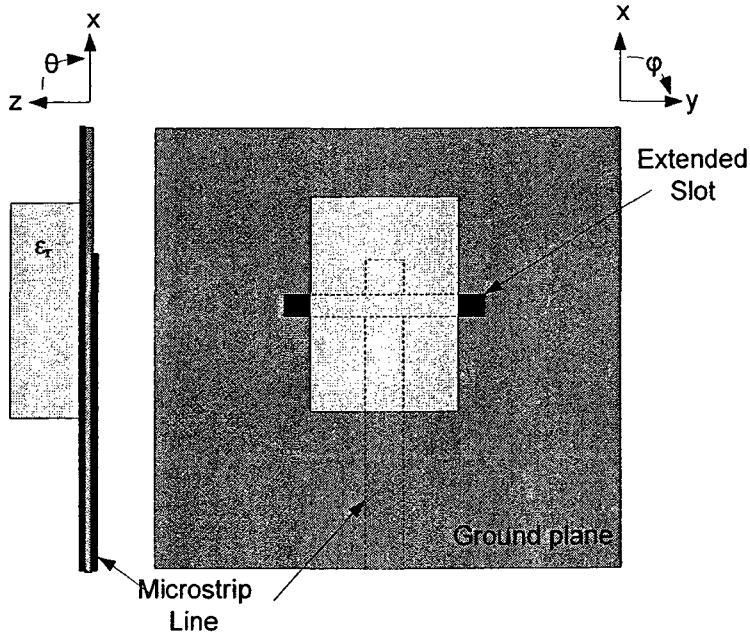

Figure 2.19: Bandwidth Enhancement by extending the slot.

As for the probe fed DRAs, the strip probe is used for wide bandwidth applications. The strip probe is used to excite two modes inside the DRA with similar radiation characteristics so that the radiation pattern is fairly constant over the entire bandwidth. For a rectangular DRA fed by a strip probe, similar to the configuration shown in Figure 2.20 [9] , the strip slot excites the $TE_{\delta 11}$ and $TE_{\delta 13}$ modes in the DRA. By adjusting the dimensions of the DRA and the strip, the two modes could be merged together and hence a broadband characteristics are achieved.

Regarding the direct microstrip feeds, the microstrip lines could be loaded by stubs to improve the impedance bandwidth.

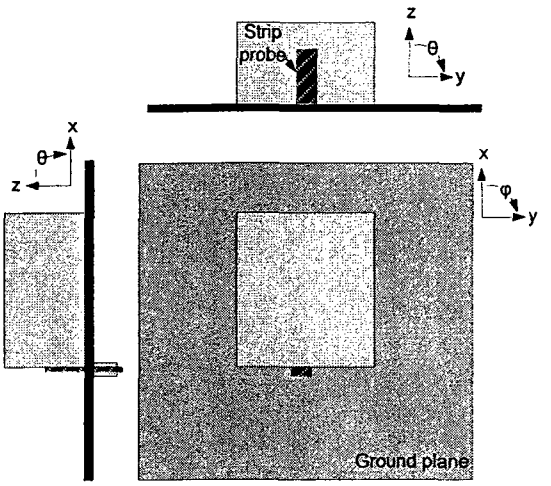

Figure 2.20: Using a strip probe for Bandwidth Enhancement.

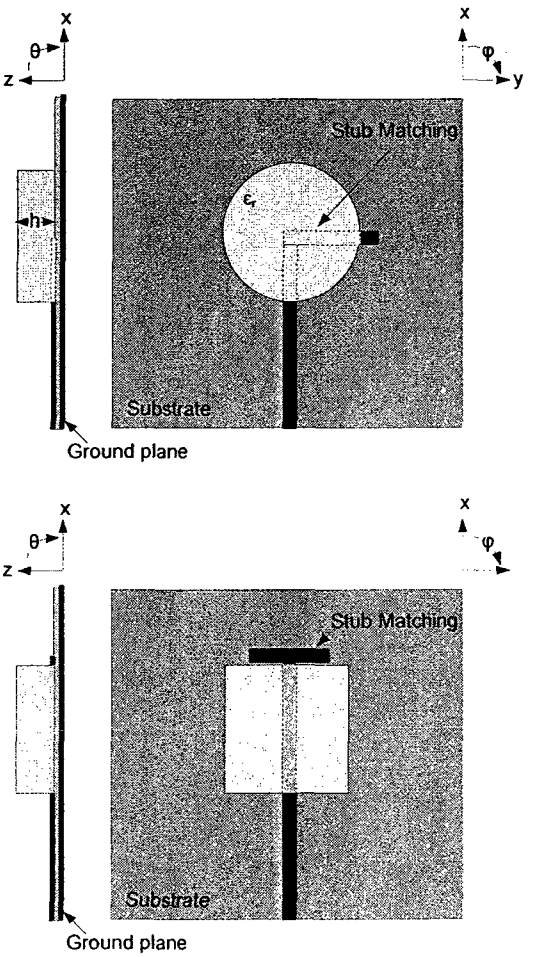

Figure 2.21: Microstrip loaded stubs for bandwidth Enhancement.

In Figure 2.21, a T-stub is used to improve the bandwidth of a rectangular DRA [7] whereas a bended stub is used to a rectangular DRA [8].

2.6.2 Multiple DRA technique

The bandwidth of DRAs depends on many parameters. The DR material used in the design and its dimensions have a strong impact on the DRA to be designed. If two or more DRAs are designed so that each DRA resonates at a particular frequency, the impedance bandwidth of the overall antenna structure will be larger than the sum of the Bandwidths if each antenna is used separately. This could only be achieved if the resonant frequency of each DRA is properly chosen [28]. There are several ways to help controlling the frequencies of each DRA so that broadband characteristics are achieved. The DRAs could be stacked, embedded, or they could be place on the same plane with one DRA is being excited and the others are electromagnetically coupled [10][12].

2.6.2.1 Stacked DRAs

In this approach, multiple DRAs with different sizes and material properties are stacked to each other and fed by a single feed mechanism. For example, a stacked Cylindrical DRA is fed by a single probe feed exciting the $HE_{11\delta}$ mode is shown in Figure 2.22. Other modes could be excited by changing the feed location. The main drawback of this technique is that the overall antenna is high in the z axes which might not be good for some applications [11] [13][14][15].

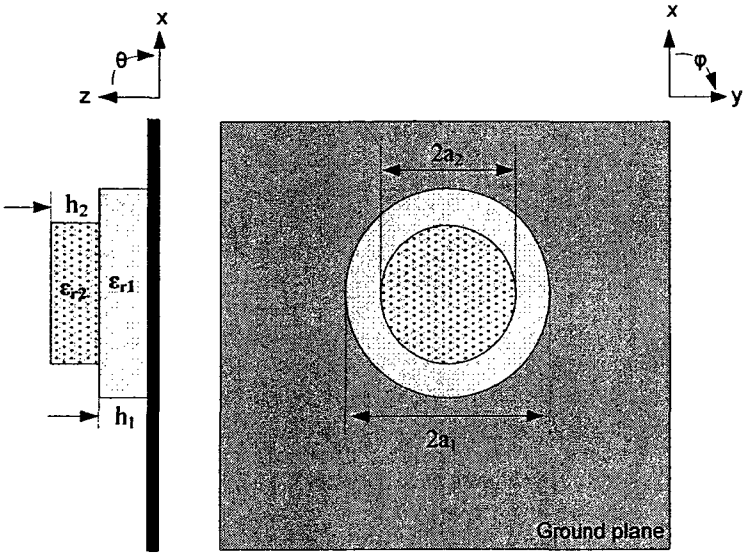

Figure 2.22: Stacked Cylindrical DRA with wideband characteristics.

2.6.2.2 Embedded DRAs

As a solution to the problem of the stacked DRAs height, DRAs could be embedded within one another. Figure 2.23 shows a small cylindrical DRA with dielectric constant (ε_{r1}), a height of (h_1), and a radius (b), is embedded inside a large Cylindrical DRA with a dielectric constant of (ε_{r2}), a height (h_2), and a radius (a) [55]. By using this technique, a wide impedance bandwidth is achieved. However, this configuration is difficult to manufacture. The easier way is to use the smaller DRA embedded in A large ring DRA [56]. This technique is easier to fabricate but the impedance bandwidth for this embedded DRA is narrower.

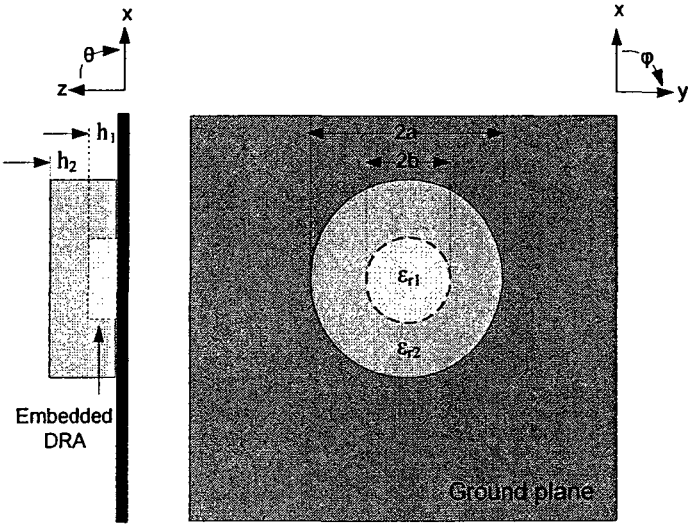

Figure 2.23: Embedded Cylindrical DRA with wideband characteristics.

2.6.3 Shaping Method

Using multiple DRAs for bandwidth enhancement is difficult to fabricate and they have complex structures. An easier technique suggests the modification of the DRA simple shapes, such as notching the DRA or altering its geometry. This section describes these techniques for bandwidth enhancement.

2.6.3.1 Conical and Stepped Inverted Pyramidal DRAs

Conical DRAs and Split-Conical DRAs are used to offer wideband characteristics. The Conical DRA shown in Figure 2.24 slightly improved the bandwidth achieved by a cylindrical DRA. If the Cone is inverted, the bandwidth is increased to almost twice the bandwidth when the cylindrical DRA is used [57].

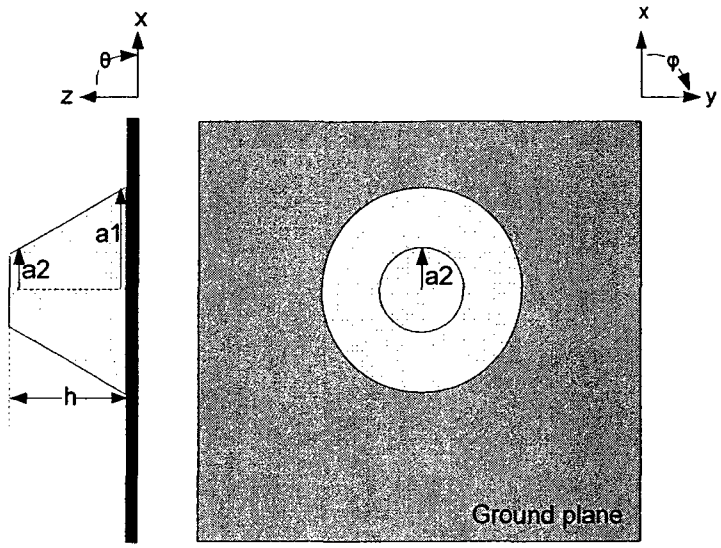

Figure 2.24 Conical DRA.

As for the split-conical DRA shown in Figure 2.25, a wider bandwidth is achieved and the radiation pattern is not constant over the entire bandwidth because of the higher order modes excited in the DRA [58].

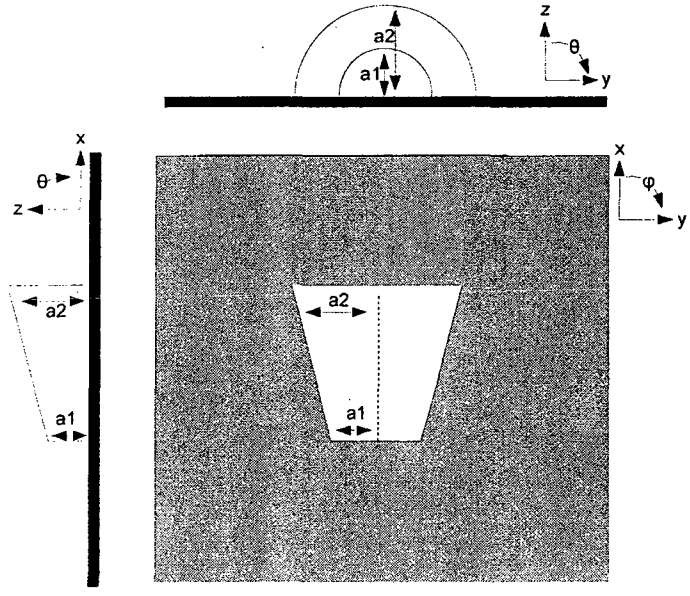

Figure 2.25 Split-Conical DRA.

An inverted stepped pyramidal DRA is also used to improve the bandwidth of the rectangular and Cylindrical DRAs. This kind of technique is shown in Figure 2.26. In contrast of the Stacked DRAs method, the inverted stepped pyramidal method uses the same DR material formed in a stepped pyramidal shape and inverted on the ground plane to offer a wider bandwidth [59][60]. The bandwidth response can be achieved by merging the resonance frequencies as these frequencies are controlled by adjusting the steps of the pyramid [58] [61].

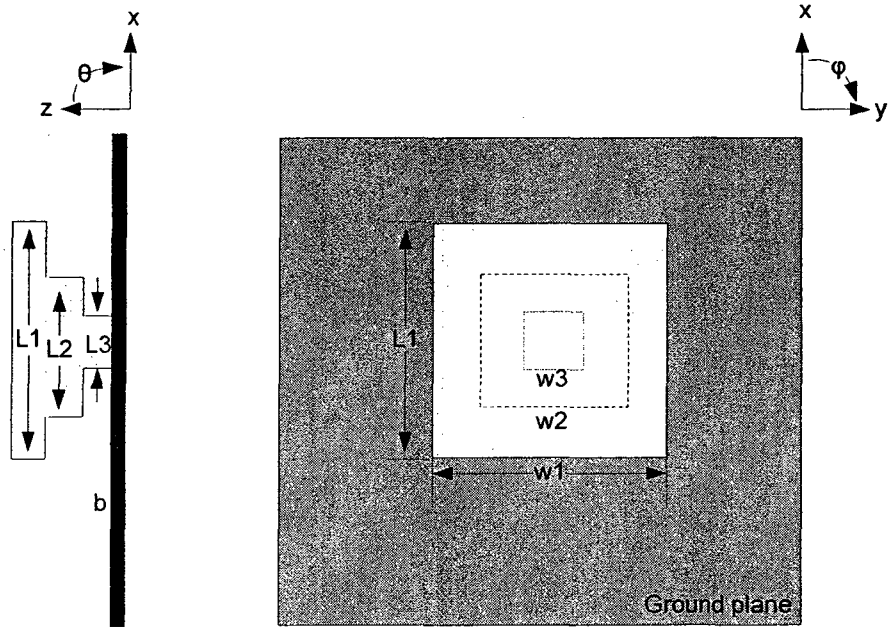

Figure 2.26 Rectangular Stepped Inverted Pyramidal DRA.

2.6.3.2 Notched DRAs

This method suggests that removing a portion of a DRA lowers the Q-factor and hence widens the impedance bandwidth. The notched rectangular DRA on ground plane is shown in Figure 2.27. The notched DRA and its image form a square hollow which

acts similar to the ring DRA. By adjusting the dimensions of L_1, and $2b_2$, a dual frequency or broadband responses can be achieved. The bandwidth of a solid rectangular DRA has been increased by introducing a notch in it [62]. Due to the height of the notch, the coupling to the DRA by using a slot is inefficient. Therefore, a high dielectric insert is added on top of the aperture operating as an impedance transformer between the microstrip line and the DRA [61]. An alternative way is to use the probe coupling to feed the antenna.

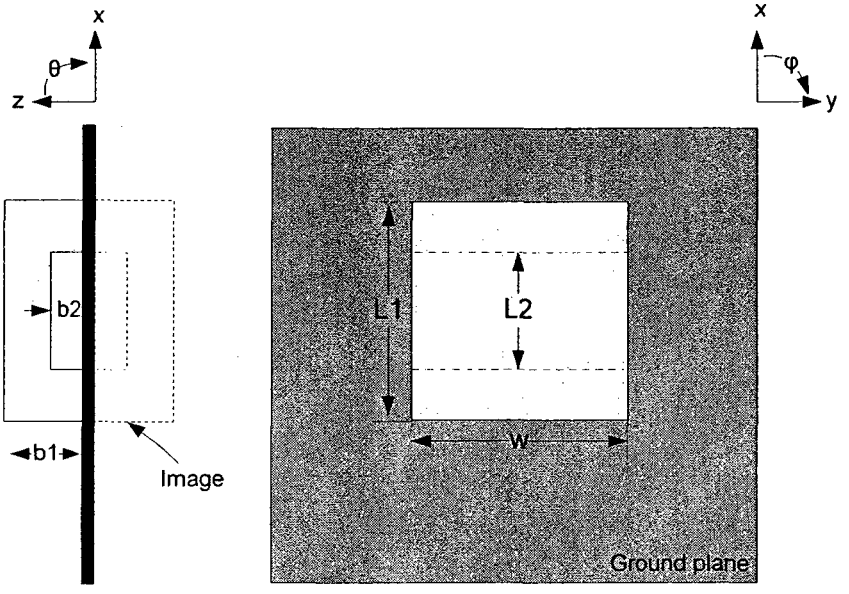

Figure 2.27 Notched Rectangular DRA.

2.6.4 Hybrid DRAs

Another approach to improve the DRA impedance bandwidth is to combine it with a batch antenna or monopole antenna. The following subsections explain these two methods.

2.6.4.1 Microstrip-DR Antenna

This technique uses a stepped microstrip feed exciting a low permittivity DRA as shown in Figure 2.28. The Q-factor of the DRA is already low as a low permittivity DR is used. As for the stepped microstrip feed, it is used as an efficient coupling mechanism to the DRA, and as a radiating part if its dimension are properly adjusted[63].

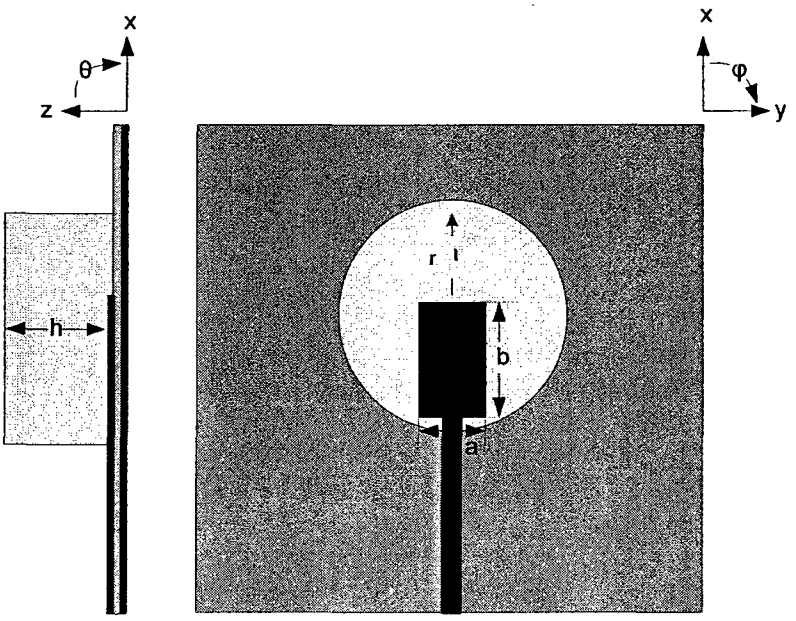

Figure 2.28 Microstrip/DR hybrid Antenna.

2.6.4.2 Monopole-DR Antenna

With the same concept used in the Microstrip/DRA hybrid antenna, a monopole antenna is combined with a ring DRA centered about the same axis as shown in Figure 2.29. The monopole operates as a quarter wavelength radiator as well as a feed for the DRA. The DRA is adjusted so that the $TM_{01\delta}$ is excited as it has the same radiation characteristics of the monopole antenna. The monopole is designed to resonate at the

lower resonant frequency whereas the DRA is designed to resonate at the upper resonant frequency to be small size [64]. By adjusting the dimensions of both antennas, a dual-band or broadband characteristics can be achieved. The air gap underneath the DRA is used to widen the bandwidth as well.

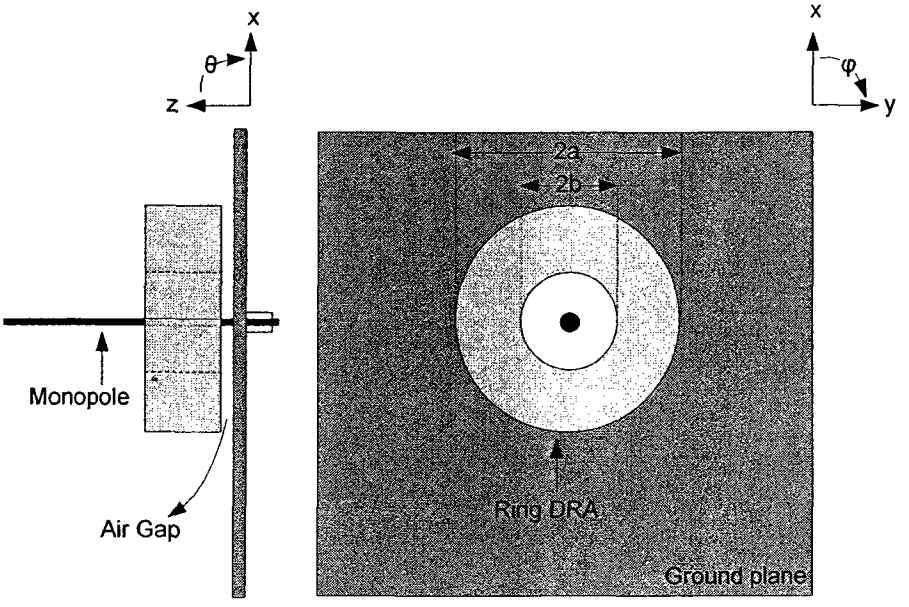

Figure 2.29 Monopole/DR Hybrid Antenna.

2.7 Numerical Techniques used with DRAs

This section presents some numerical techniques used to predict the input impedance of the DRAs as predicting the input impedance gives a precise design to the DRA at that specific input impedance excited by a particular feed.

2.7.1 Frequency Domain Techniques

Method of Moments (MoM) and Finite Element Method (FEM) have been used to analyze the DRAs. In the MoM, the antenna is discretize into small segments. The currents on the segments due to a known incident field is represented by unknown coefficients. Therefore these coefficients can be solved by using standard numerical techniques. Once the currents are determined, the DRA input impedance can be calculated. The MoM is used with DRAs by introducing equivalent currents. This method requires fine segments for an accurate solution [65]. Therefore, it is not a desirable solution in the DRA case.

For the FEM, the DRA, the ground plane, and the entire volume surrounding the DRA are discretized to small tetrahedrons. Although this increases the computational size of the problem, the FEM has many advantages over the MoM. The advantage of using the FEM is that it doesn't require the formulation of equivalent currents and hence it can be applied to arbitrary geometries [28][66]. Many commercial software packages like Ansoft HFSS [19] are based on FEM.

2.7.2 Time Domain Techniques

In the time domain analysis, there have been two methods applied to analyze the DRA; the finite difference time domain (FDTD) method [67], and the transmission line method (TLM) [68]. In these techniques, the entire volume around the DRA is discretized. Small

cubes are used instead of tetrahedrons. When discretizing the curved geometries, stair-stepping effect should be taken into account for a proper modeling. In the time domain methods, a wideband pulse is used to excite the DRA, and then the solution is transformed into frequency domain determining the input impedance over a wide frequency range. In the case of frequency domain methods, the input impedance calculations are repeated at each frequency to obtain the input impedance over the frequency range which is a time consuming process [28]. Finite Integration technique (FIT) is a generalization of the FDTD method. It uses the integral form of Maxwell's equations instead of the differential ones [69]. CST Microwave Studio [20] is based on the FIT.

Chapter 3

Theoretical Background for DRA Design

3.1 Introduction

This chapter is devoted for the design procedure, and the theoretical fundamentals which the design is based on. To easily design a DRA for a particular application, the resonant natural resonant frequency should be known. The Q-factor, and the modes of operation has to be known because the antenna bandwidth is directly affected by the Q-factor, and the radiation patterns are affected by the excited modes inside the DRA. The resonant frequency and the Q-factor are easy to find in the case of rectangular and hemispherical Dielectric resonator antennas by solving the transcendental equations presented in chapter 2. However, for the cylindrical DRA, the numerical solutions are not of ease as in the case of the hemispherical and rectangular DRAs. The following section describes an accurate method to start the general design of cylindrical DRAs. The design of the half-cylindrical DRA, which is the main topic of this thesis, will be developed based on the design of the cylindrical DRA. Section 3.3 presents the design of the rectangular DRA as it will be partly used in this thesis. The hemispherical DRA design is not covered because it is out of the scope of this thesis.

3.2 Design of Cylindrical DRA

In general, design of a cylindrical DRA requires a preliminary knowledge of the natural resonant frequencies and Q-factors of the antenna. To know the natural frequency, the feed network is removed. Then, numerical methods are applied to examine the frequencies at which the DRA have a response without any excitation. These frequencies are the resonant frequencies. One of the numerical methods used to evaluate the natural frequencies is described in [70]. However, these techniques are complicated and time consuming for antenna designers. Therefore, many other alternatives have been presented as those in [5] and [27]. In [5], the resonant frequencies and Q-factors are computed for the cylindrical dielectric resonator antenna at three dielectric constants and then curve fit equations have been estimated for the resonant frequencies and Q-factors in terms of radius to height ratio (a/h), and dielectric constant (ε_r). In [27], empirical formulae are expressed to estimate the resonant frequencies and the Q-factors of the cylindrical DRAs. These expressions are the basic design formulae in this thesis.

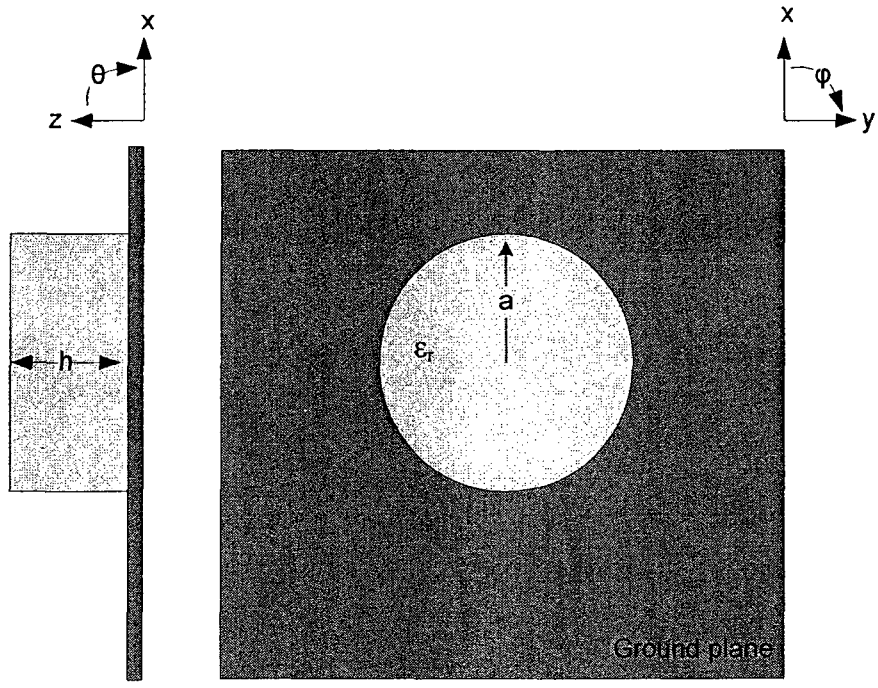

Figure 3.1: Geometry of the cylindrical DRA in the side and the top views.

The empirical equations in [27] are used to estimate the resonant frequencies and the Q-factors of the first four modes; $TE_{01\delta}$, $HE_{12\delta}$, $TM_{01\delta}$, and $HE_{12\delta}$.

For the $TE_{01\delta}$ mode, the expressions for the resonant frequency and the Q-factor are giving as [28]:

$$k_0 a = \frac{\left(2.1439 + 0.6604\chi + 0.2733\chi^2 - 0.1919\chi^4\right)}{\varepsilon_r^{0.475}} \tag{3.1}$$

$$Q = 5.72\chi\left(1 + 18.387\chi^{-0.3795} e^{-1.64\chi}\right) \tag{3.2}$$

where $\chi = \frac{a}{2h}$ (3.3)

For the $TM_{01\delta}$ mode, the expressions are given as:

$$k_0 a = 0.8945 \frac{\left(1+3.017\chi^{0.881}+e^{0.962-1.6252\chi}\right)}{\varepsilon_r^{0.45}} \tag{3.4}$$

$$Q = 10.9\chi\left(1+217.96\chi^{3.4796}e^{-3.67\chi}\right) \tag{3.5}$$

For the $HE_{11\delta}$ mode, the expressions are given as:

$$k_0 a = \frac{\left(1.6+0.513\chi+1.392\chi^2-0.575\chi^3+0.088\chi^4\right)}{\varepsilon_r^{0.42}} \tag{3.6}$$

$$Q = \chi\varepsilon_r^{1.2}\left(0.01893+2.925e^{-2.08\chi(1-0.08\chi)}\right) \tag{3.7}$$

For the $HE_{12\delta}$ mode, the expressions are given as:

$$k_0 a = \frac{\left(3.72+0.4464513\chi+1.392\chi^2-0.575\chi^3+0.088\chi^4\right)}{\varepsilon_r^{0.42}} \tag{3.8}$$

$$Q = \varepsilon_r^2\left(0.068-0.388\chi+0.0064\chi^2+0.0007e^{\chi(37.59-63.8\chi)}\right) \tag{3.9}$$

The above equations are used for the design of a cylindrical DRA with a radius (a) and a height (h).

As the frequency and the Q-factor are known. The radiation pattern should also be known. The near field and the far field distributions are important to compute as the near field helps to determine the appropriate excitation method and the far field distribution

helps to determine if the DRA to be designed is useful for a particular application in terms of the radiation patterns. Figures 3.2 to 3.5 show sketches of the field distributions inside the DRA in two perpendicular planes. In chapter two, more details of the excitation methods are presented for DRAs with different shapes. In this section, more concern is devoted to the cylindrical DRA.

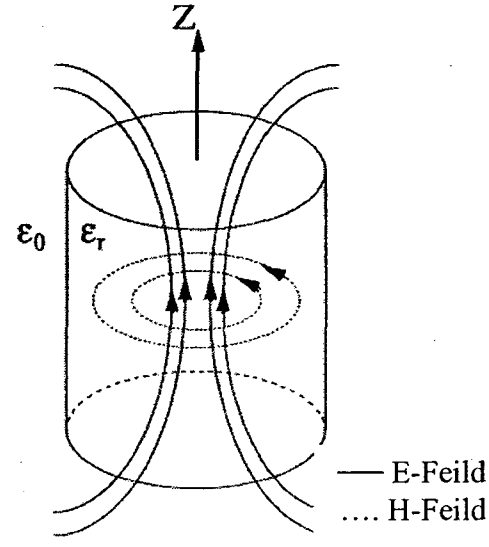

Figure 3.2: Field distribution of the $TM_{01\delta}$ mode. [27]

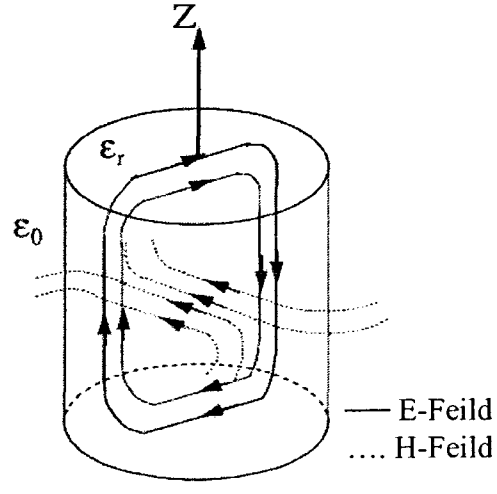

Figure 3.3: Field distribution of the $HE_{11\delta}$ mode.[27]

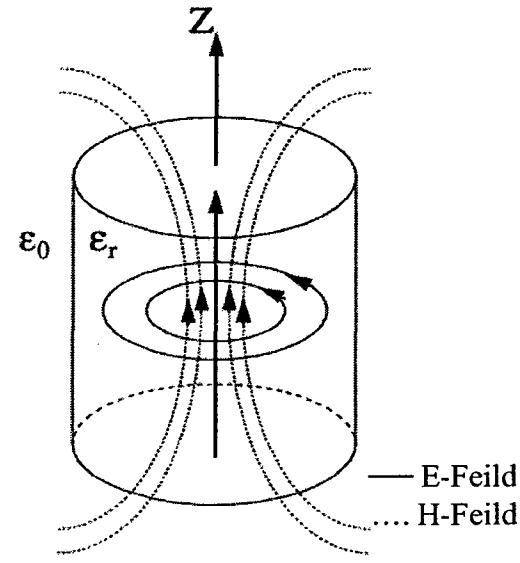

Figure 3.4: Field distribution of the TE_{018} mode. [27]

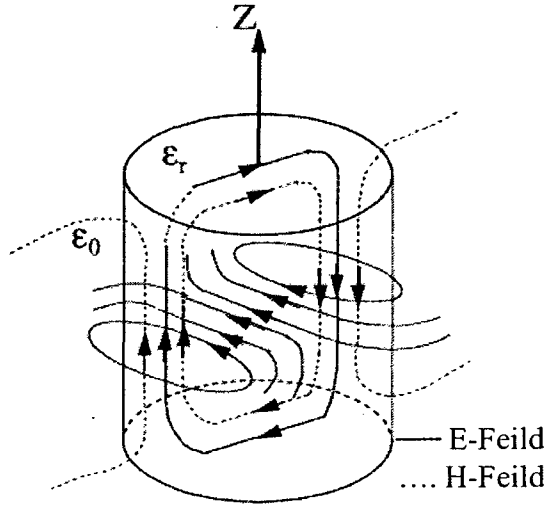

Figure 3.5: Field distribution of the HE_{128} mode. [27]

The Electric fields could be excited by an electric probe along the Electric field lines or a narrow slot along the magnetic field lines [27]. In the sketches shown above, the

modes can be excited if a conducting plane is placed in the plane of the magnetic field lines.

The $TM_{01\delta}$ and $HE_{11\delta}$ can be excited if a perfectly conducting plane intersects the cylinder from the middle of its height as the field distributions are not disturbed. The $TM_{01\delta}$ mode radiates like a short electric monopole whereas the $HE_{11\delta}$ radiates like an electric dipole parallel to the ground plane, a quarter wavelength monopole above the ground plane, or a half wavelength narrow slot in the ground plane.

The $TE_{01\delta}$ and $HE_{12\delta}$ can be excited if the DRA is placed on a magnetic conductor plane which is physically unrealizable. An electric conductor could be used to split the DRA disc along the Z axis. The $TE_{01\delta}$ radiates like $HE_{01\delta}$, and the $HE_{11\delta}$ radiates like the $TM_{01\delta}$ mode. It has been reported in [5] that the rate of change in the resonant frequency in the $TE_{01\delta}$ and $HE_{12\delta}$ with respect to the DRA aspect ratio (a/h) is less than that for the $TM_{01\delta}$ and $HE_{11\delta}$. Therefore, the bandwidth seems to be wider in the case of the $TE_{01\delta}$ and $HE_{12\delta}$ modes. These two modes are excited by using the half-cylindrical DRA the reason why the half-cylindrical over a ground plane is chosen in this thesis.

3.3 Design of Half-Cylindrical DRA

This section presents a detailed procedure for the half-cylindrical DRA design as it is the main topic of this thesis. The design equations given in section 3.2 will be used in this section as well. The half-cylindrical DR is placed on a ground plane and the $TE_{01\delta}$

mode is to be excited. The aperture slot is used as a feeding mechanism because it has similar radiation characteristics as the DRA in the $TE_{01\delta}$ mode. Equations 3.1 to 3.9 applies in this case except that h is replace by 2h (the half-cylinder height) because when the cylinder is placed on the ground plane, it is image introduced the image of h, but in this case, the cylinder is divided by an electric conductor along z-axis as shown in Figure 3.6. Referring to Figure 3.6, the radius (a) is the same in all cases, h becomes 2h as the ground plane in the xy plane is removed. Accordingly the value of χ in equation 3.3 becomes

$$\chi = \frac{a}{h} \tag{3.10}$$

where a/h is the aspect ratio of the half-cylindrical DRA and it should not have very small values nor very high values.

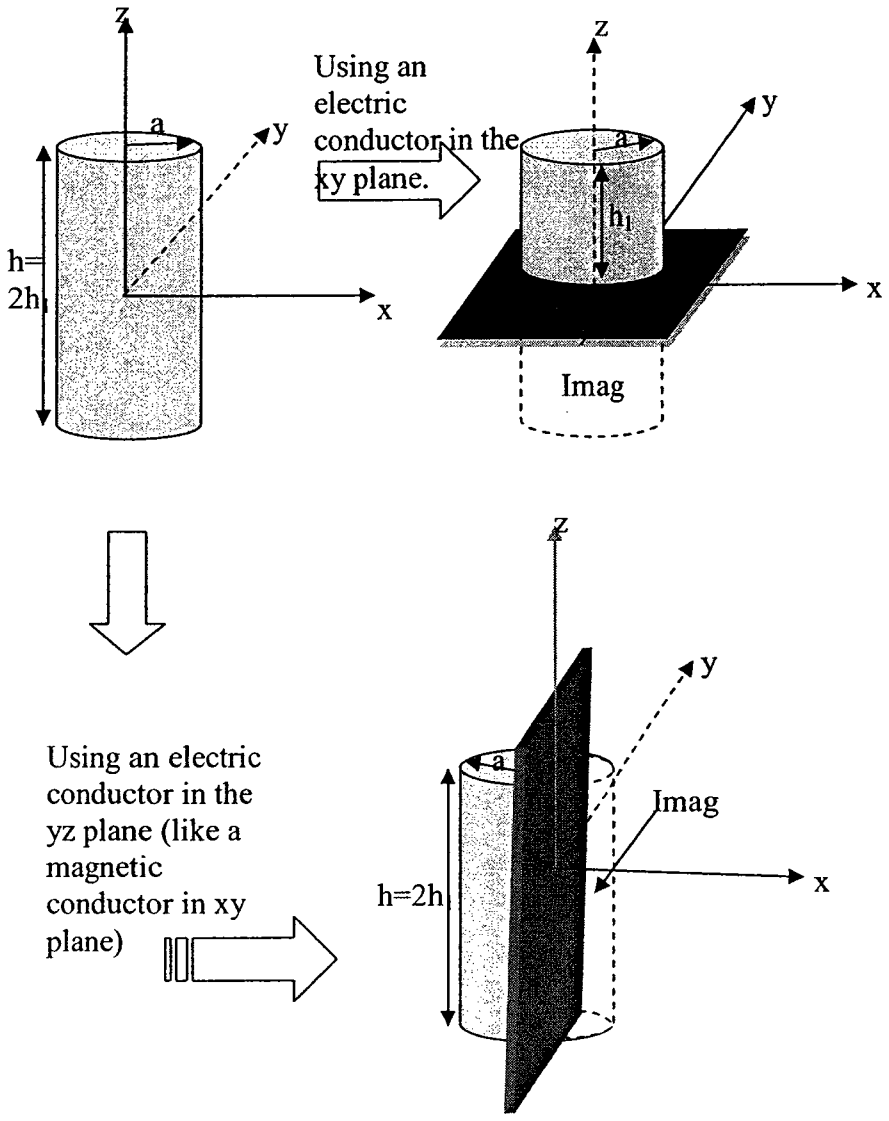

Figure 3.6: Half-cylindrical DRA and Image Theory.

As a result of this process, the design of the half cylindrical can be started by using the equations 3.1,3.2, and 3.10. A value of a/h is assumed and substituted in equation 3.1 to find (k_0a) from which the resonant frequency can be approximated by

$$k_0 a = \frac{f_{GHz} h_{cm}(a/h)}{4.7} \Rightarrow f_{GHz} = \frac{4.7(k_0 a)}{h_{cm}(a/h)} \qquad (3.11)$$

As for the coupling mechanism, the aperture slot is to be used. The slot is to be narrow to avoid the unwanted radiations from the slot. The inner slot is approximated as $\lambda_g/2$ [6].

where $$\lambda_g = \lambda_0 / \sqrt{\varepsilon_{eff}} \tag{3.12}$$

and the effective permittivity is estimated as,

$$\varepsilon_{eff} = H_{total} \Big/ \left(\frac{a}{\varepsilon_r} + \frac{t}{\varepsilon_s} \right) \tag{3.13}$$

$$H_{total} = a + t \tag{3.14}$$

where (a) is the radius of the half-cylinder, (t) is the substrate thickness, ε_s and ε_r are the relative permittivity values of the substrate and the Dielectric Resonator respectively as shown in Figure 3.7.

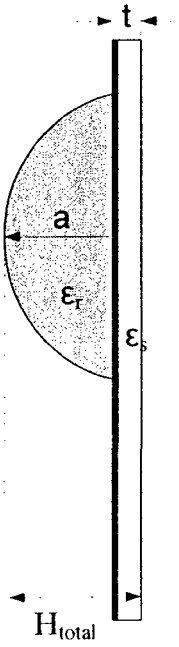

Figure 3.7: Side view of the half-cylindrical DRA.

The inner slot is to be surrounded by a U-shaped slot for more coupling and to improve the antenna bandwidth. Simulation using HFSS [19] has to be done to optimize the antenna for the improved antenna characteristics.

The last part of the design is the microstrip line as the line width (W_f) can be calculated from the width to substrate thickness (t) ratio given by the following equation [71]

$$\frac{W_f}{t} = \begin{cases} \dfrac{8e^A}{e^{2A}-2} & for \quad {}^{W_f}\!/_{t} < 2 \\ \dfrac{2}{\pi}\left[B-1-\ln(2B-1)+\dfrac{\varepsilon_s-1}{2\varepsilon_s}\left\{\ln(B-1)+0.39-\dfrac{0.61}{\varepsilon_s}\right\}\right] & for \quad {}^{W_f}\!/_{t} > 2 \end{cases} \tag{3.15}$$

$$A = \frac{Z_0}{60}\sqrt{\frac{\varepsilon_s+1}{2}} + \frac{\varepsilon_s-1}{\varepsilon_s+1}\left(0.23+\frac{0.11}{\varepsilon_s}\right), \text{and} \quad B = \frac{377\pi}{2Z_0\sqrt{\varepsilon_s}} \tag{3.16}$$

where Z_0=50 Ω. The microstrip line length is extended underneath the slot by a quarter wavelength distance from the edge ($\Delta L_f = \frac{\lambda_g}{4}$) of the slot to improve the impedance matching. The microstrip line is shown in Figure 3.8 demonstrating all the dimensions used in equations (3.15) and (3.16).

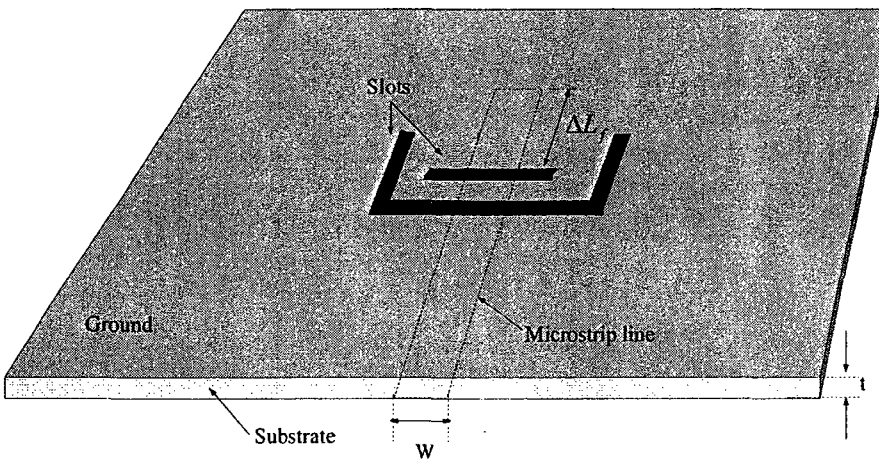

Figure 3.8: The microstrip line for the DRA.

3.4 CAD tools for DRA simulation

The design formulae explained in section 2.3 are useful for estimating the size of the DRA to be designed at a particular frequency. Using full wave-based CAD tools such as Ansoft HFSS and CST microwave studio offers precise designs and accurate results for DRA parameters.

3.4.1 Ansoft High Frequency Structure Simulator (HFSS)

Ansoft HFSS is a frequency domain technique software package. The finite element method (FEM) is used to solve Maxwell's partial differential equations describing an electromagnetic problem subject to proper boundary conditions. The entire volume is discretized into a large number of tetrahedra which is called the tetrahedral mesh or the

finite element mesh. At the vertex of each tetrahedron, the field components tangential to the three edges at each vertex are stored. The normal vector field at the midpoint of the edges is also stored. These stored values are used to estimate the electric and magnetic fields inside the tetrahedra. Maxwell's equations are formulated from the field quantities in the tetrahedral and transformed to matrix equations that is solved by numerical methods. A denser mesh of small discretizations could be used for more precise solution.

Ansoft HFSS can be used to simulate any problem in 2 or 3 dimensions at a single frequency or over a frequency band. Ansoft HFSS is used in this thesis to simulate the DRA for the return loss and the radiation patterns. Animated plots of the fields could also be displayed in three dimensions.

3.4.2 CST Microwave studio

CST microwave studio is used as another simulation tool together with HFSS to check the accuracy of numerical results. CST is based on the Finite integration technique (FIT) with the Perfect Boundary Approximation (PBA) [69]. The FIT is a generalization of the Finite-Difference Time-Domain (FDTM) and it also has links with the FEM [69]. In this method, the integral form of Maxwell's equations in time domain are discretized instead of the differential ones. The PBA mesh has an excellent convergence properties. The simulation doesn't require a huge memory to be carried out. Accordingly, using the PBA mesh is suitable to simulate the large structures as the simulated results can be obtained in a very short time. Comparing the PBA with the staircase mesh and the

tetrahedral mesh, it is considered the best one in terms of the low memory requirements[69].

The tetrahedral mesh also has excellent convergence properties but it requires large memory and a long computing time if large structures are to be simulated. As for the staircase mesh, it is suitable for simple structures without curved structures as it will not converge in a reasonable computing time[68].

The simulated results in the following chapter are obtained using HFSS. CST microwave studio is just used to verify the first step antenna design to make sure that the fabricated antennas will be operating as efficient as possible.

Chapter 4

DRA Design Results

4.1 Introduction

This chapter provides the design methodology of three proposed DRAs for WLAN applications. The design procedure is the same for all of the antennas. There have been several techniques to improve the bandwidth of DRAs which have been discussed in detail in chapter 2. Image theory has been applied to design a compact DRA. To make this compact DRA broadband, an aperture slot is used to excite the antenna. A parasitic U shaped slot is part of feeding network for more coupling to the DRAs. The utilization of the U slot has shown a very strong effect on the DRAs impedance bandwidth. Moreover, it offers more design flexibility for a better antenna characteristics. This chapter presents the broadband half-cylindrical DRA, the half cylindrical DRA backed by a rectangular DRA, and the compact DRA with an elliptical half cylinder geometry. These three proposed antennas utilize the same excitation mechanism. The design formulae presented in chapter three have been used as a first design step. The following flow graph explains the design methodology of the three proposed antennas. See Figure 4.1.

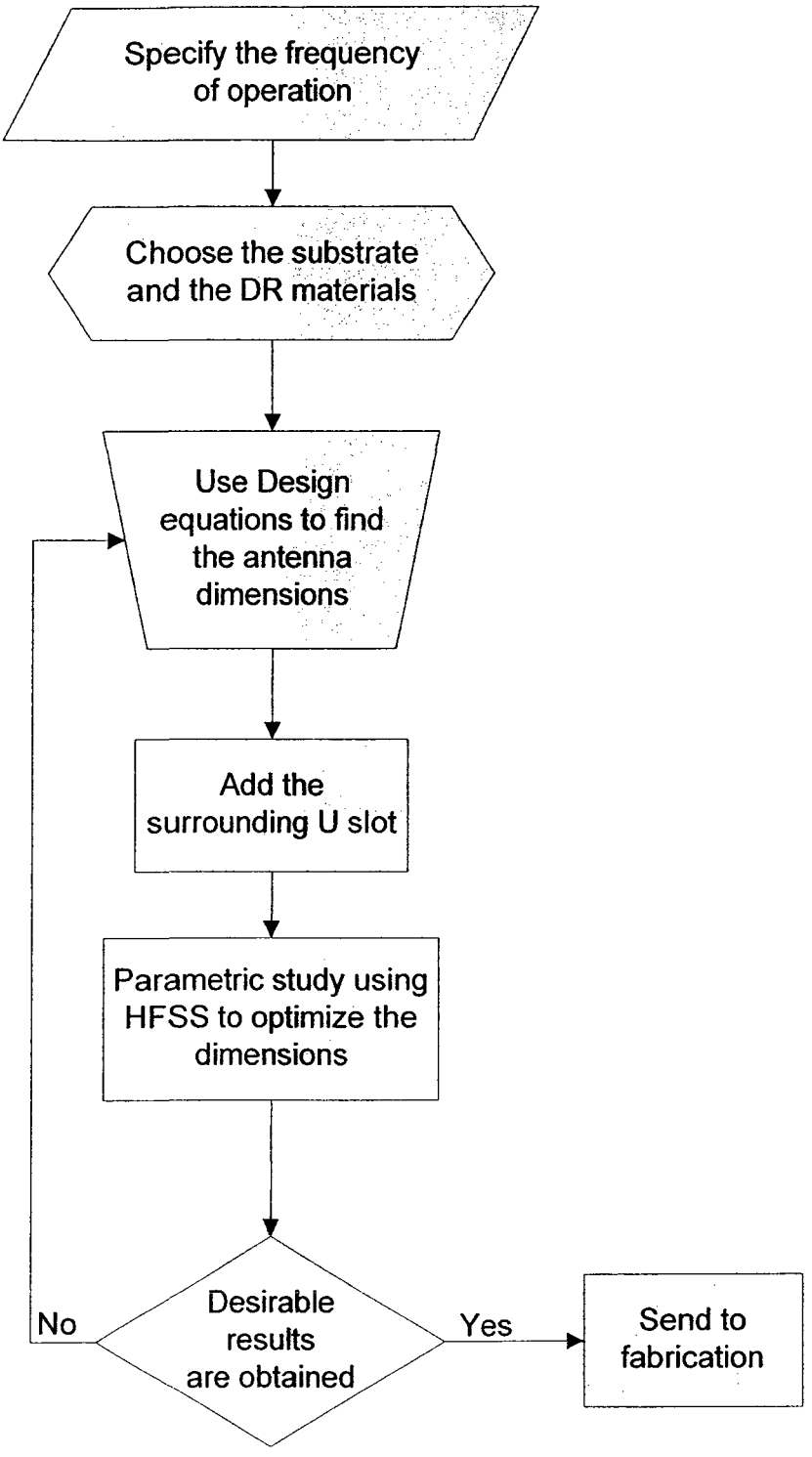

Figure 4.1 DRA Design Methodology.

4.2 Broadband Half-cylindrical DRA

The geometry of the proposed DRA in this section is a half cylinder with a height (H=15mm), and a radius of (R=7.25mm). The antenna geometry is shown in Fig.4.2. The dimensions of the half cylinder are first adjusted using the equations in chapter 3. The DR is mounted on a 30×30 mm^2 ($0.57\lambda_0 \times 0.57\lambda_0$) where λ_0 is the free space wavelength at the center frequency. The antenna is excited by an aperture coupling slot and a parasitic U shaped slot. The DR is placed at 5.75mm from the center of the ground plane along the x axis which is the location of the high current distribution[7].

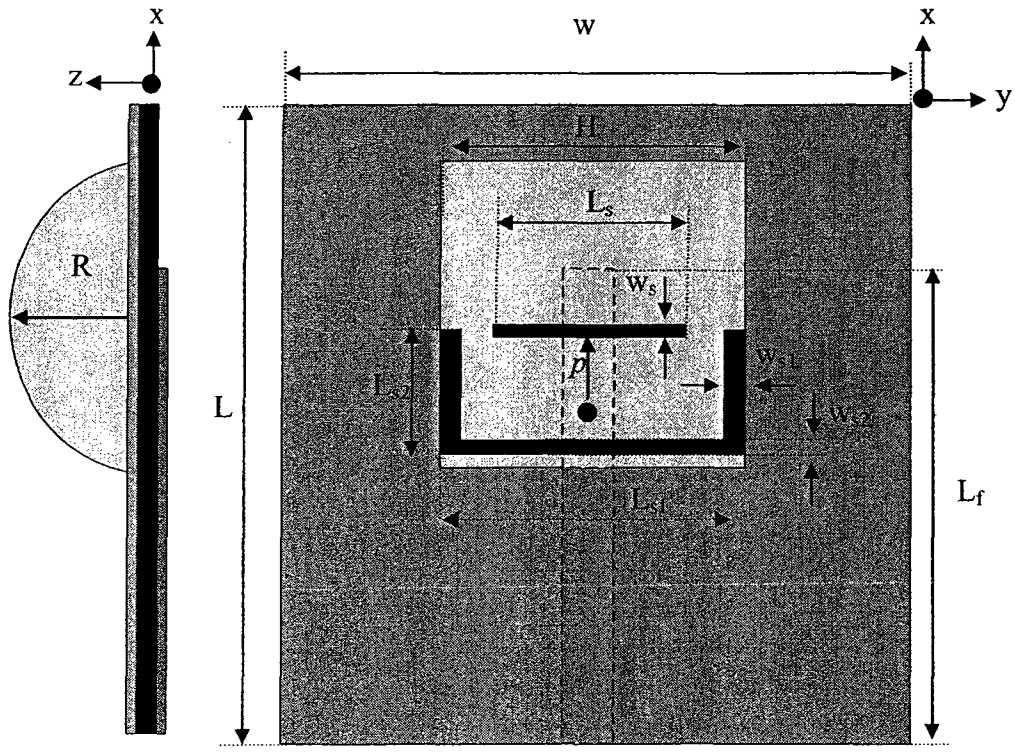

Figure 4.2 The half-cylindrical DRA structure.

The DR material is Rogers RO3010 ™ with ε_r=10.2, and a dielectric loss tangent of 0.0035. The planer substrate material is Rogers RT/Duroid 5880 ™ with ε_s=2.2, a loss tangent of 0.0009, and thickness of 0.767 mm.

4.2.1 Design Verification

After a preliminary estimation of the antenna size using the equations given in chapter 3, the DRA is optimized using HFSS [19]. The design model is exported to CST Microwave Studio [20] to make sure that the antenna is operating in the desirable band. Figure 4.3 shows the results obtained from these software packages. It also shows the measured results as it can be observed that there is a frequency shift because of the air gap between the DRA and the ground plane. The simulation time of full wave numerical techniques is not very long because the small antenna size. However, for a larger problem size, high frequency techniques such as Geometric Theory of Diffraction should be used [74].

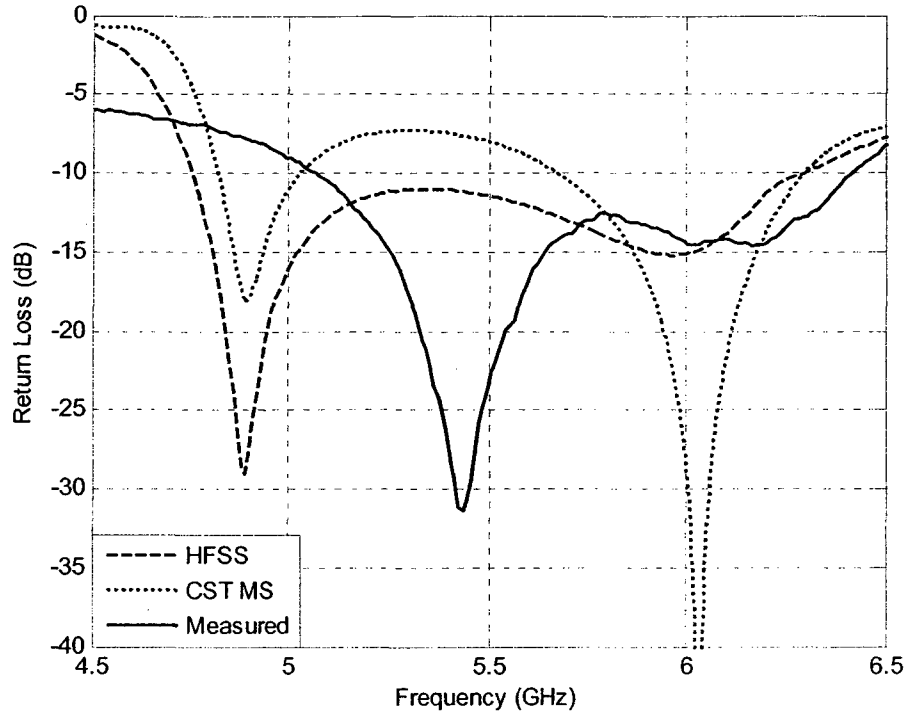

Figure 4.3 Return Loss results from HFSS and CST compared to the measured S_{11}.

4.2.2 Parametric Study

The effect of each design parameter is to be investigated in this section. Ansoft HFSS [19] is used for the parametric study as it uses the FEM with the tetrahedral mesh which is accurate because the simulation is repeated at each frequency. In time domain methods, a wideband pulse is used to excite the DRA, and the solution is transformed to the frequency domain to determine the input impedance over a wide band of frequencies [28].

4.2.2.1 Microstrip length (L_f)

As shown in Fig.4.3, the DRA has two resonance frequencies controlled by the microstrip line length. They could be controlled such that the antenna has a dual frequency response. If the microstrip line length is increased, the two resonance frequencies merge together to get the broadband characteristics.

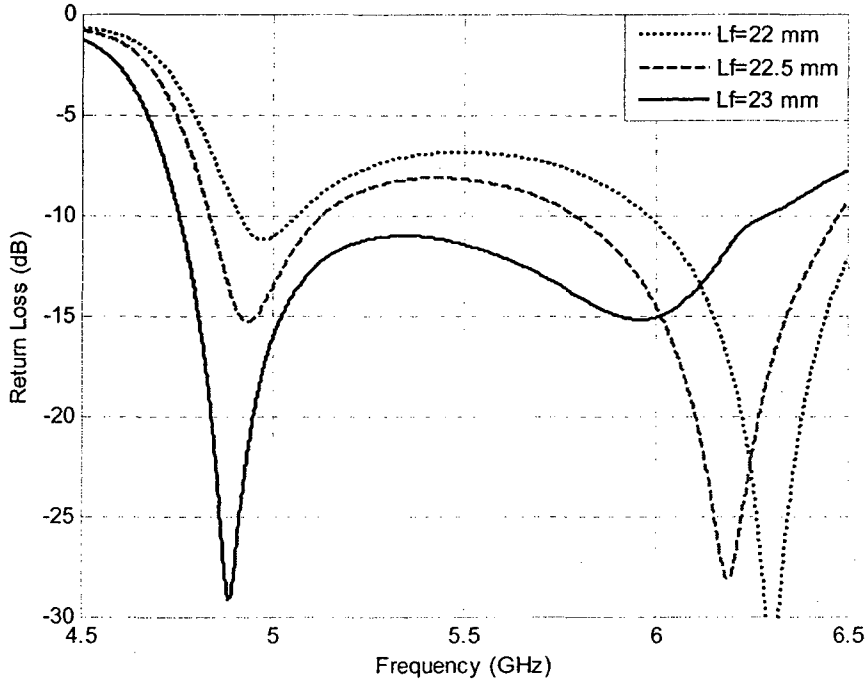

Figure 4.4: Effect of microstrip length.

4.2.2.2 The inner slot length (L_s)

The aperture coupling slot length is changed to figure out its effect on the antenna behaviour. As it is a part of the feed network, it has a considerable effect on the antenna radiation. For the slot width it has to be less than a quarter wavelength to avoid the back

lobes in the resulting radiation pattern. As shown in figure 4.5, the second resonance is highly affected by changing the slot length which indicates that the inner slot is mainly used to excite the DR to be resonant at 6 GHz.

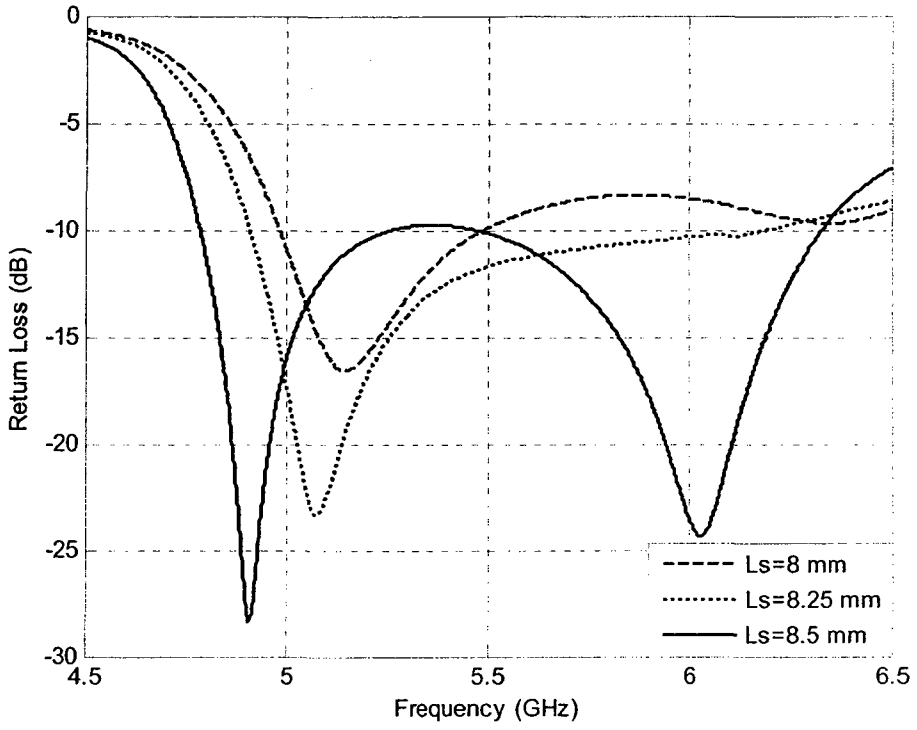

Figure 4.5 Effect of the inner slot length.

4.2.2.3 The shift of the inner slot position (p) from the center of the DRA

The inner slot position is a very critical factor. This slot should be placed at the strongest current distribution. Fig.4.5 illustrates the effect of the shift along the x axis from the center of the antenna. As it is shown, at an offset point of (p=5mm) from the antenna center, the coupling to the DR is improved. It is also noticed that the position of the inner slot mainly affects the high resonance frequency (6 GHz).

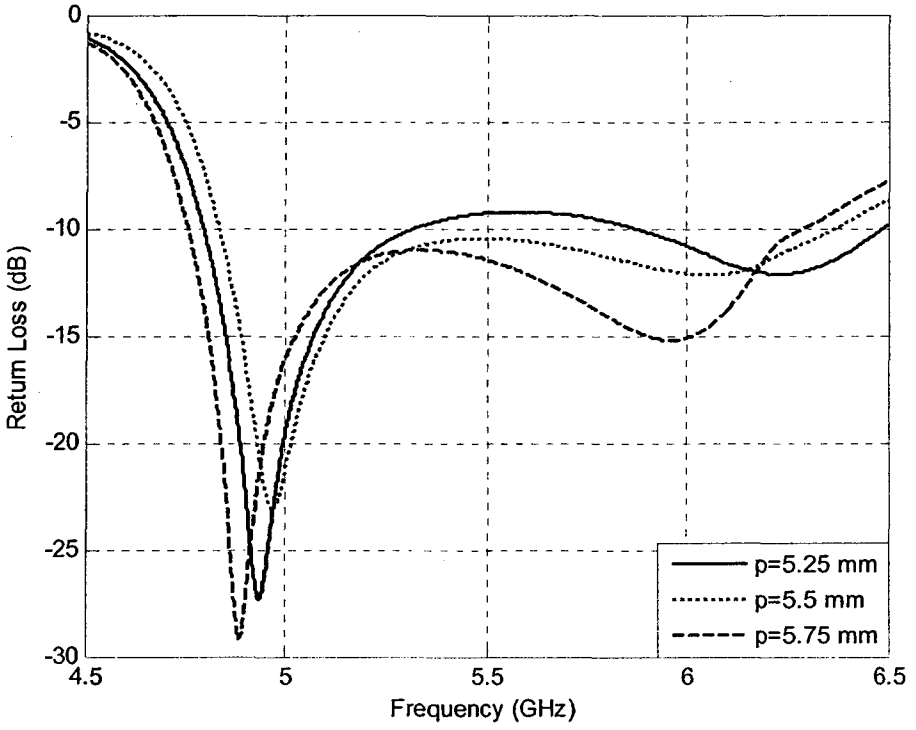

Figure 4.6: Effect of the inner slot position.

4.2.2.4 The horizontal arm of the U slot (L_{s1})

The horizontal arm of the parasitic U-slot is used to increase the coupling to the DRA. However , the width of this arm should be kept small enough to avoid the back lobes in the radiation patterns. It could be noticed in Fig.4.7 that the horizontal arm resonates the first resonance frequency (4.9GHz). The second resonance frequency is also affected because of the strong resonance that occurs at the first resonance (4.9 GHz). However, when the arm is adjusted to 15.5 mm, the antenna performance is improved.

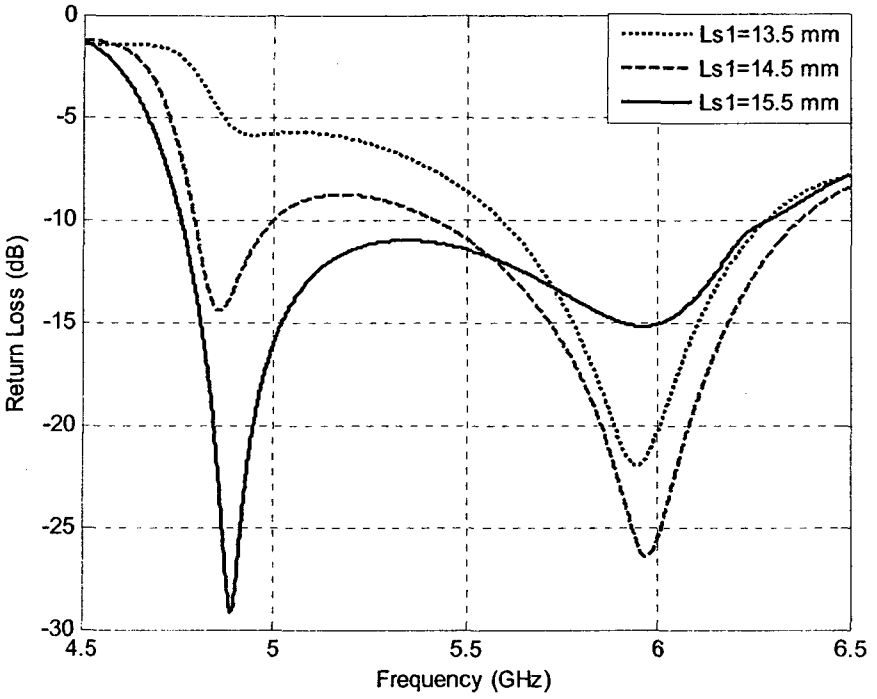

Figure 4.7 Effect of the horizontal arm of the U slot.

4.2.2.5 The symmetrical parallel arms of the U-slot (L_{s2})

As shown in the above sections, the inner rectangular slot is used to excite the DR to be resonant at the high resonance frequency and the horizontal arm of the U shaped slot is used to resonate at the lower resonant frequency. The parallel symmetrical arms of the U slots are used to control the antenna matching and to adjust the two resonances to achieve the broadband characteristics. As it can be noticed in Fig.4.8 that the resonance frequencies merge together as the two symmetrical arms of the U-slot are increased.

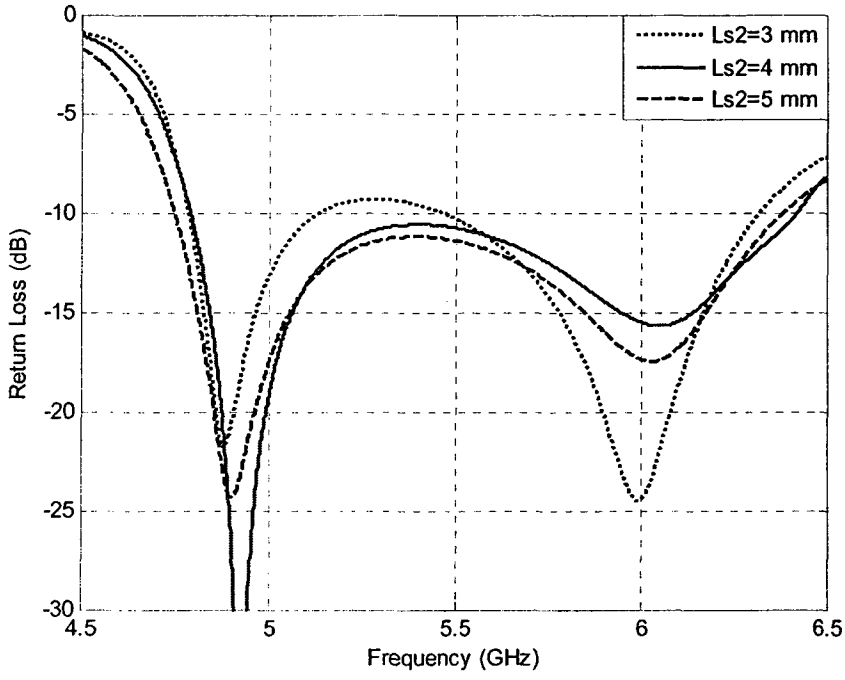

Figure 4.8 Effect of the parallel arms of the U slot.

4.2.3 Impedance Bandwidth of the fabricated DRA

After the parametric study, the return loss of the optimized antenna is obtained by Ansof HFSS [19] and the antenna has been fabricated. Figure 4.9 shows the fabricated half-cylindrical DRA. The antenna return loss for the fabricated antenna is shown in Figure 4.10. The simulated return loss obtained from HFSS and CST Microwave studio are plotted on the same graph for comparison. As it can be noticed, the fabricated antenna operates properly in the frequency range from 5 GHz to 6.4 GHz. It is noticed that there is a frequency shift from the simulated results. This is attributed to the air gap between the dielectric resonator and the ground plane.

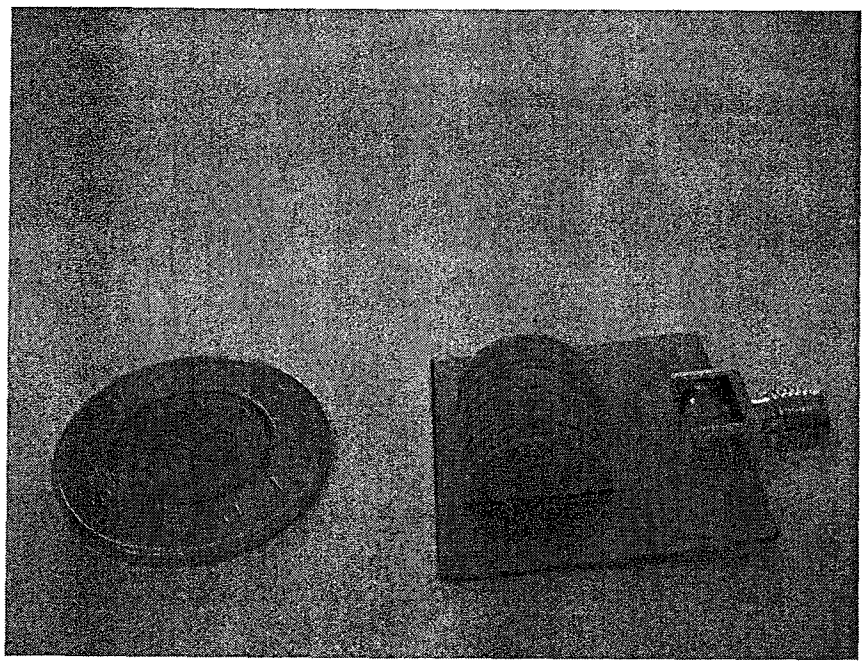

Figure 4.9 A picture of the half-cylindrical DRA.

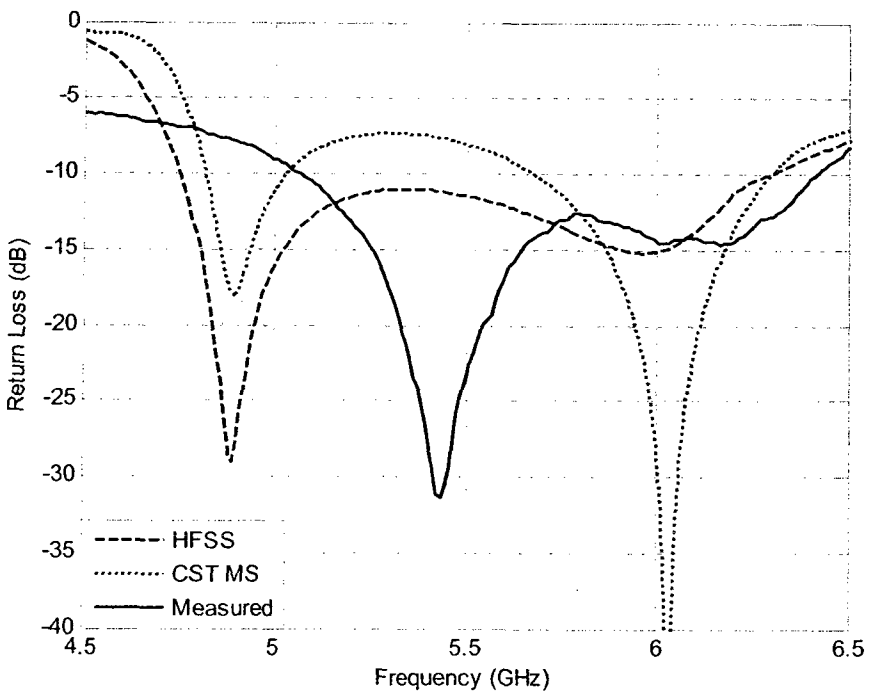

Figure 4.10 Measured and simulated return loss for the half-cylindrical DRA.

4.2.4 Antenna Gain

Although the antenna size is small, the antenna has reasonable gain values over the operating frequency band. The antenna maximum gain is 6 dBi which is in the central band of frequencies whereas at the edge frequencies, it has a value of 4 dBi. The antenna gain over the entire impedance bandwidth is shown in Figure 4.11.

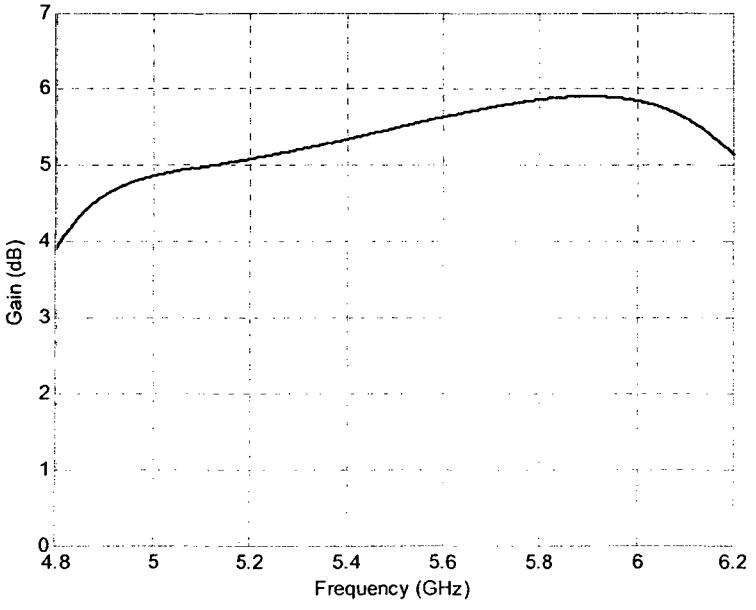

Figure 4.11: Gain of the Half-Cylindrical DRA.

4.2.5 Antenna Radiation patterns

The radiation patterns in the azimuth (H) and elevation (E) planes are shown in Figures 4.12, and 4.13. The radiation patterns in both planes are examined at three different frequencies within the operating bandwidth. The cross-polarized fields are also examined as the antenna is immunized against these fields.

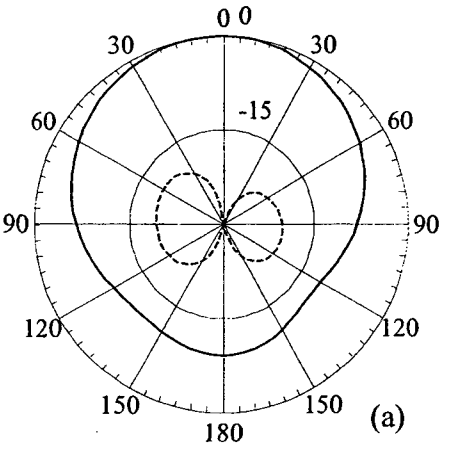

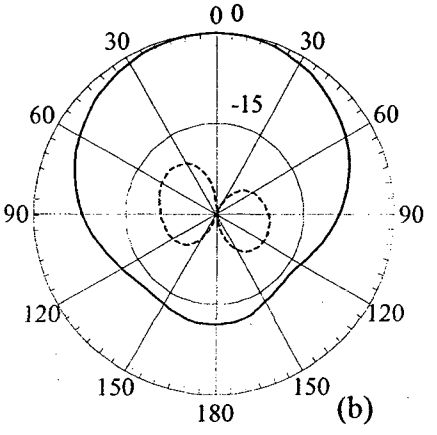

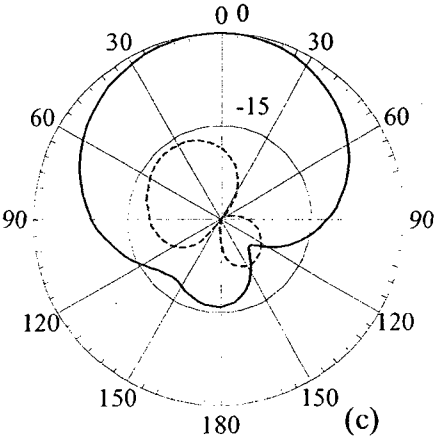

Figure 4.12 Co-polarized (solid), and cross-polarized (dash) fields in the H (yz) plane, (a) f=4.8 GHz , (b) f=5.2GHz , (c) f=5.8GHz.

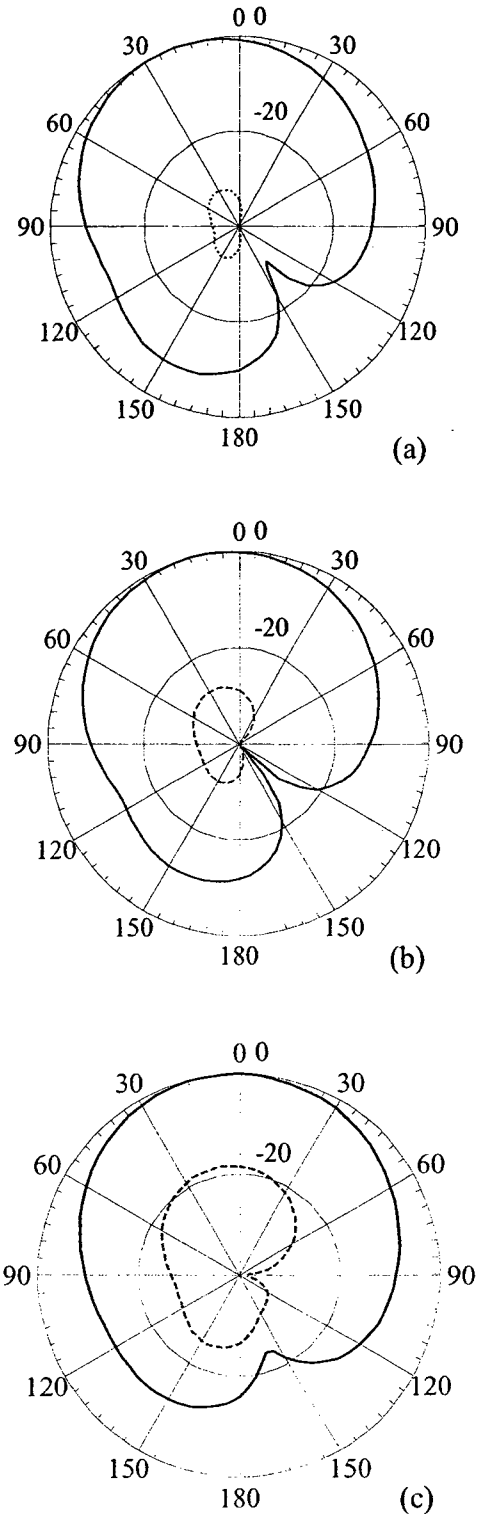

Figure 4.13 Co-polarized (solid), and cross-polarized (dash) fields in the xz (E) plane, (a) f=4.8 GHz , (b) f=5.2GHz , (c) f=5.8GHz.

The radiation patterns in the H-plane (E_φ) and the E-plane (E_θ) obtained from HFSS and CST microwave Studio at 5.8 GHz are plotted on the same plot. The cross polarized fields are also plotted as their level is less then -15 dB in the H-plane and less than -20 dB in the E-plane. This can be noticed in Figure 4.14. As it can be noticed that the patterns are similar in both planes.

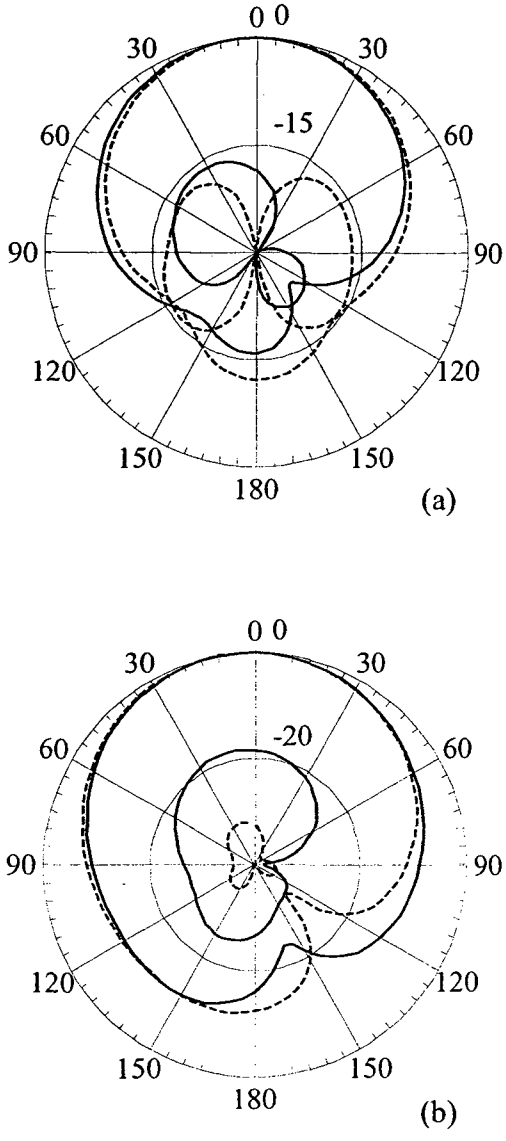

Figure 4.14 Radiation patterns obtained from HFSS (solid), and CST (dash) in (a) H-plane, and (b) E-plane.

The measured radiation patterns in H and E-planes are plotted in Figure 4.15. The simulated results are plotted on the same graph. It can be observed that there is a spillover in the radiation patterns because of the finite ground plane. The electromagnetic scattering from the edges of the ground plane caused this kind of radiation. However, this can be accepted as it is not very large.

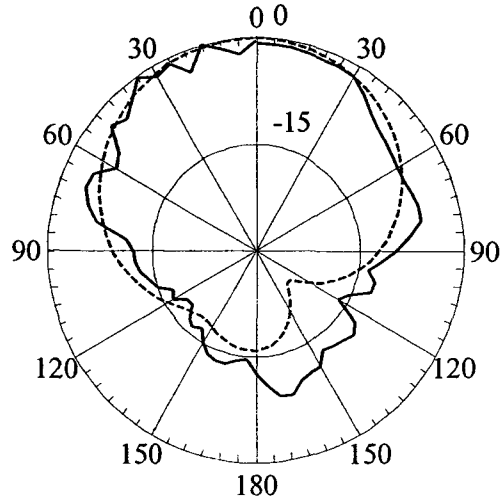

(a)

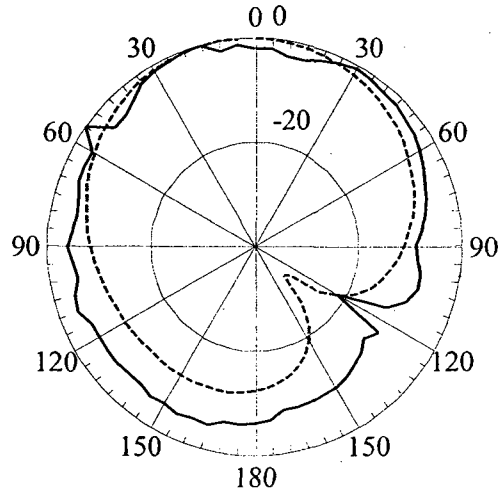

(b)

Figure 4.15: Measured (solid) and simulated (dash) radiation patterns in (a) H-plane, and (b) E-plane.

4.3 Half-cylindrical DRA backed by a rectangular dielectric resonator (RDR)

The Dielectric Resonator Antenna (DRA) presented in this section is composed of two geometries. The first geometry is a half cylinder with a height of H=15.5 mm along y-axis, radius R=7 mm in the x-z plane. The second geometry is a rectangular Dielectric resonator along the cylinder in the xy plane, and a height of z=3 mm along the z-axis. The antenna is to be fed by aperture coupling slot with $L_s \times w_s$= 7 mm × 1 mm in the xy plane. The surrounding U slot has a horizontal arm of $L_{s1} \times w_{s1}$ = 17 mm × 0.5 mm, and parallel arms of $w_{s2} \times L_{s2}$= 0.5 mm ×8 mm, all in the xy plane on a 30×25 mm^2 ground plane. The antenna is excited by a 50Ω microstrip line. The substrate material is made of Rogers RT/Duroid 5880 with ε_r=2.2, loss tangent of 0.0009 and the DRA is made of Rogers RO3010 ™ with ε_r=10.2, and a loss tangent of 0.0035. See Figure 4.16 [75].

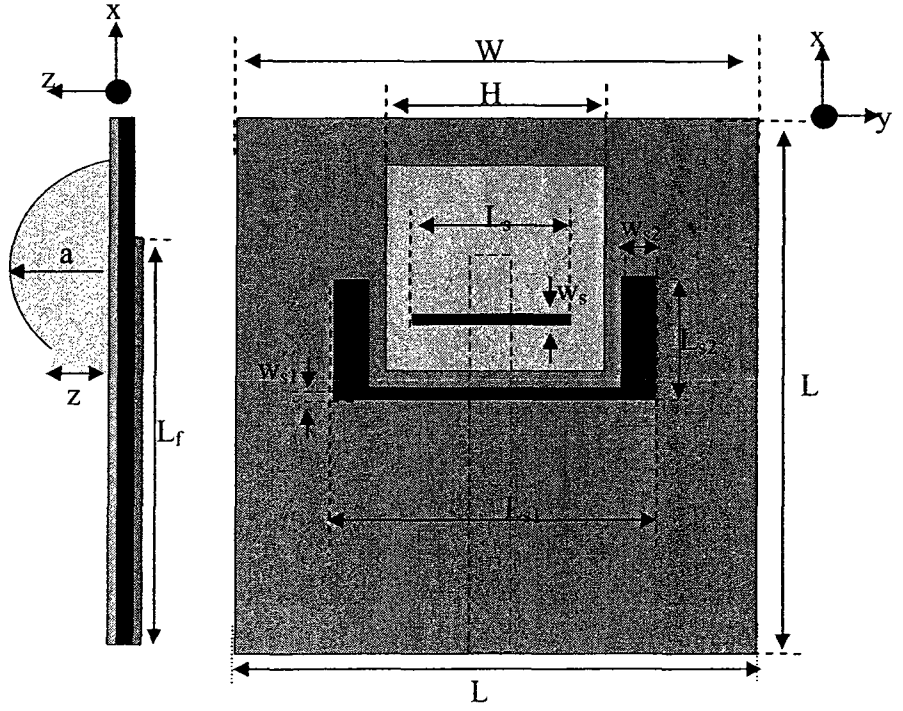

Figure 4.16 Half-cylindrical DRA backed by a rectangular DRA.

4.3.1 Design Verification

As it has been done in the first model of the Half-cylindrical DRA presented in section 4.2, CST is also used to verify the results obtained from HFSS in the optimization process. The results obtained from both software packages are plotted on the same graph which is shown in Figure 4.17. The antenna is resonant over the band of interest (5.2/5.8 GHz). As it can be noticed, there is 200 MHz frequency shift because each tool uses a different numerical technique as HFSS uses the FEM and the time domain solver is used in CST for these results.

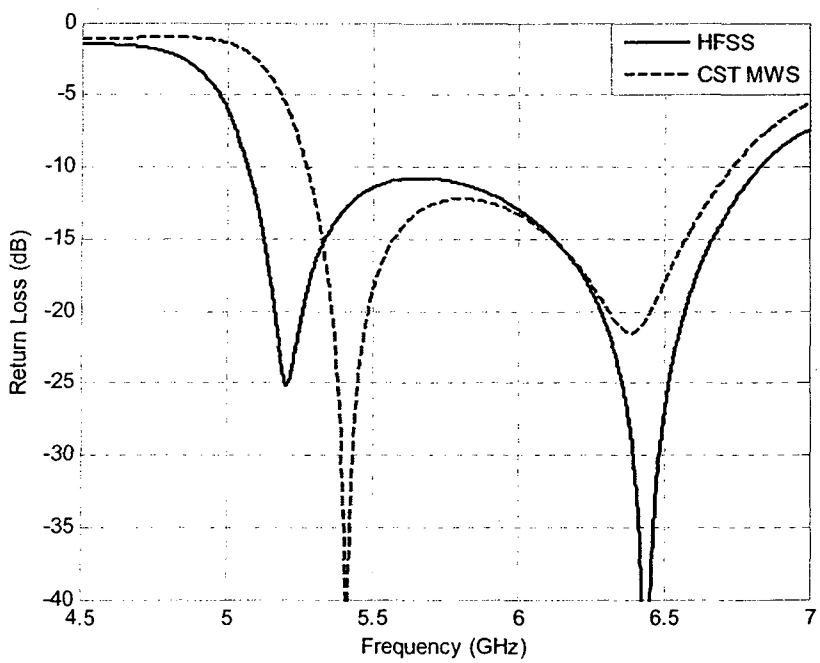

Figure 4.17 Return Loss obtained from HFSS and CST.

4.3.2 Parametric study

As this antenna has a similar geometry to that of the antenna presented above. The parametric study will be done to the size of the rectangular DRA. However, another parametric study will be applied to the parasitic U-shaped slot because it is not underneath the DRA in this case. It is around the DRA as shown in Figure 4.15.

4.3.2.1 Effect of the rectangular DR size

The half-cylinder is backed by a rectangle made of the same dielectric material. The height of this rectangle affects the matching of the antenna as the width of this rectangle is kept the same as the half-cylinder height. As shown in Figure 4.18, the bandwidth is improved when the rectangle height z=3 mm is adjusted.

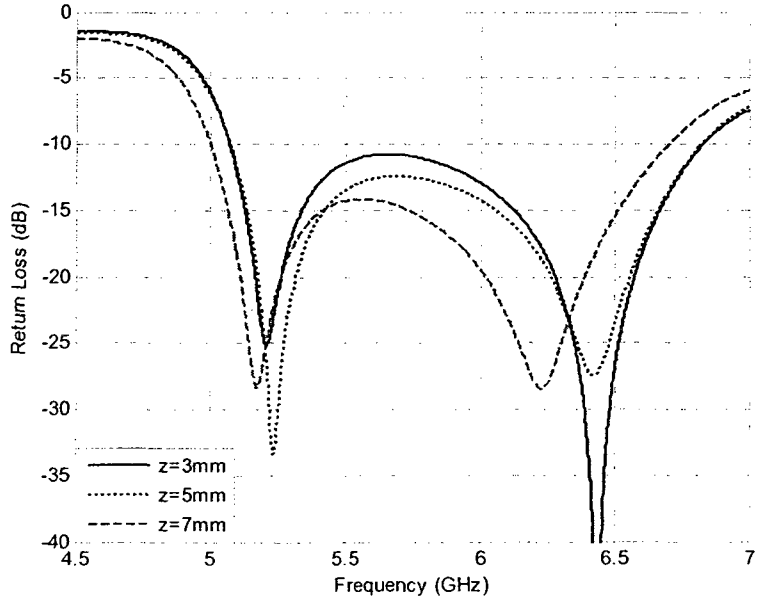

Figure 4.18 Effect of the rectangle size on the DRA performance.

4.3.2.2 Effect of the horizontal arm of the U slot (L_{s1})

As the horizontal arm of the U-slot increases, the upper resonance frequency disappears which means that the radiation at the upper resonance frequency is due to the U slot. This can be shown clearly in Figure 4.19.

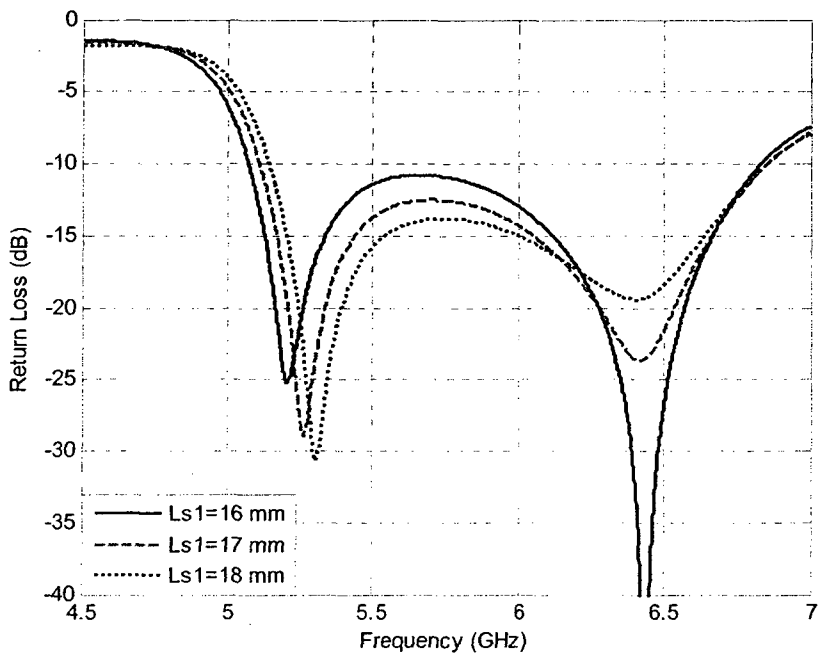

Figure 4.19 Effect of the horizontal arm of the U slot.

4.3.2.3 Effect of the symmetrical parallel arms of the U slot (L_{s2})

The effect of this parameter is shown in Figure 4.20. It is noticed that as if the U arms are increased, the best matching could be obtained. Therefore, the parallel arms of the U slot are used to control the matching of the antenna.

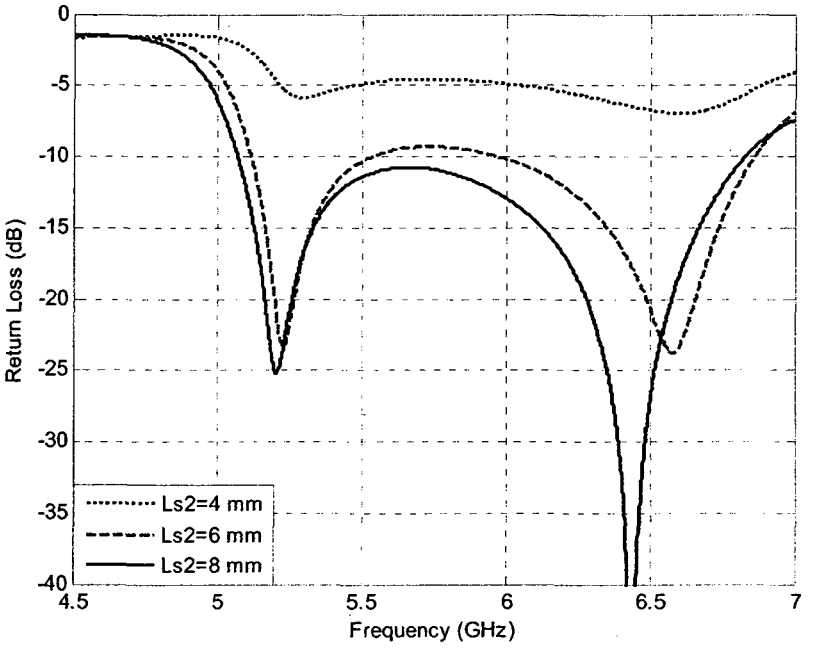

Figure 4.20: Effect of the parallel arms of the U slot.

4.3.3 Measured Impedance Bandwidth

After the parametric study is done, the return loss of the optimized antenna is obtained by Ansof HFSS [64] and the antenna has been fabricated. Figure 4.21 shows the fabricated half-cylindrical DRA. The antenna return loss for the simulated antenna is shown in Figure 4.22. The results for the fabricated antenna are shown on the same graph for comparison. As it can be noticed, the antenna operates properly in the frequency range from 4.8 GHz to 6.6 GHz or 31% centered around f_r=5.7 GHz. The frequency shift is due to the air gap between the DRA and the ground plane.

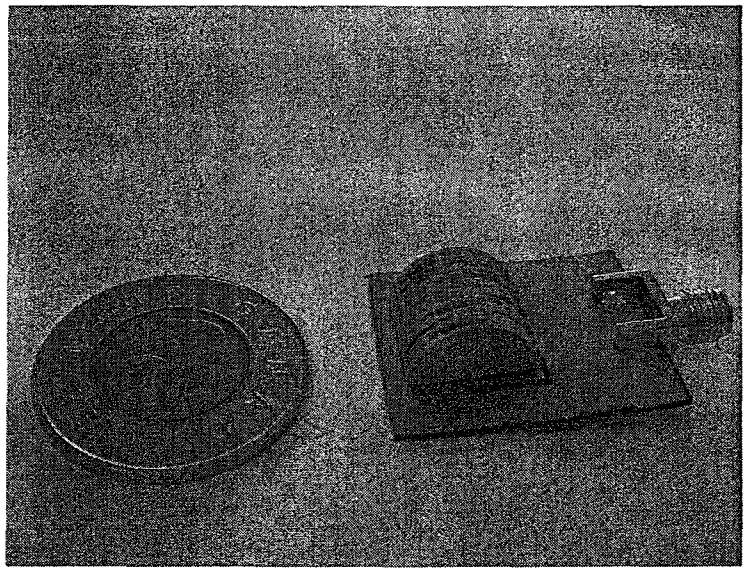

Figure 4.21: A picture of the fabricated half-cylindrical DRA backed by a rectangular dielectric resonator.

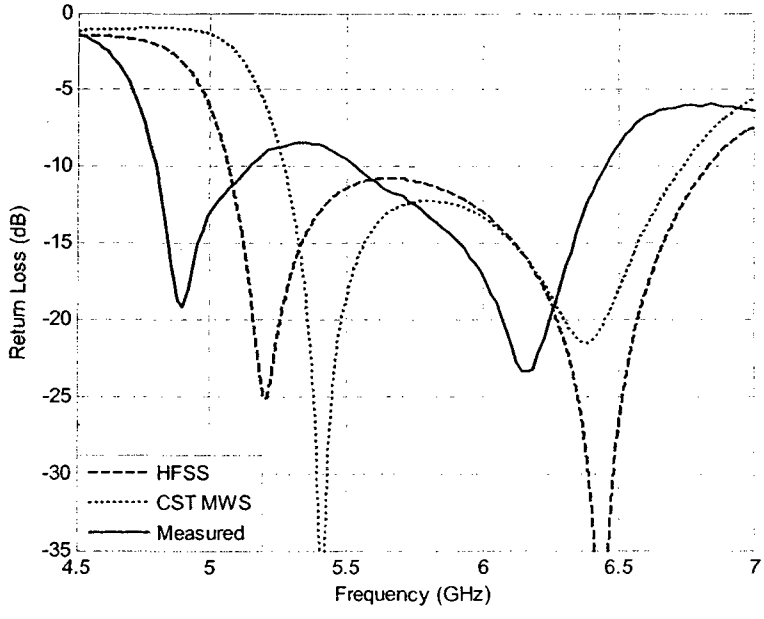

Figure 4.22: Simulated and measured return loss of the half-cylindrical DRA backed by a rectangular dielectric resonator (RDR).

4.3.4 Antenna Gain

The size of this antenna is decreased if compared to the DRA presented in section 4.2. Although the antenna size is smaller, the antenna maintains the same gain values over the operating frequency band. The maximum gain value is 5.8 dBi. The smallest gain value is 4 dBi. See Figure 4.23.

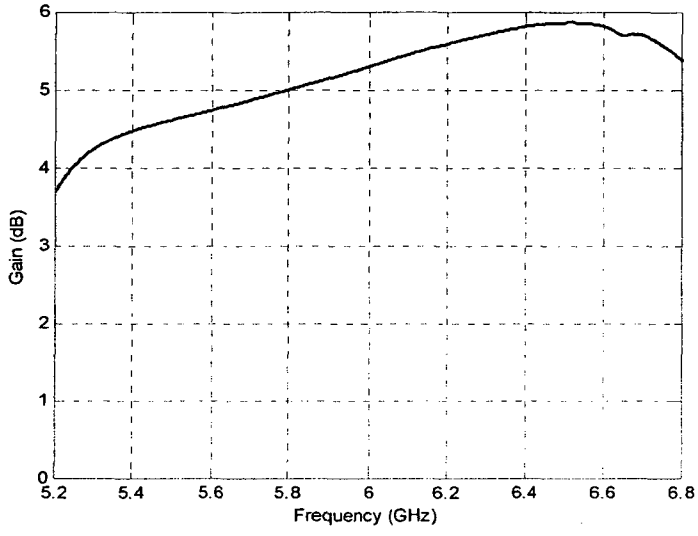

Figure 4.23: Gain of the half-cylindrical DRA backed by a rectangular dielectric resonator (RDR).

4.3.5 Antenna Radiation patterns

The antenna radiation patterns are computed at different frequencies in the E and H planes. The antenna has the broadside radiation characteristics in the H-plane, and quasi-broadside radiation characteristics in the E-plane because of the radiation of the two slots

adds to each other in the direction θ=30°. It is also noticed that the antenna has low cross-polarized fields level, see Figures 4.24 and 4.25.

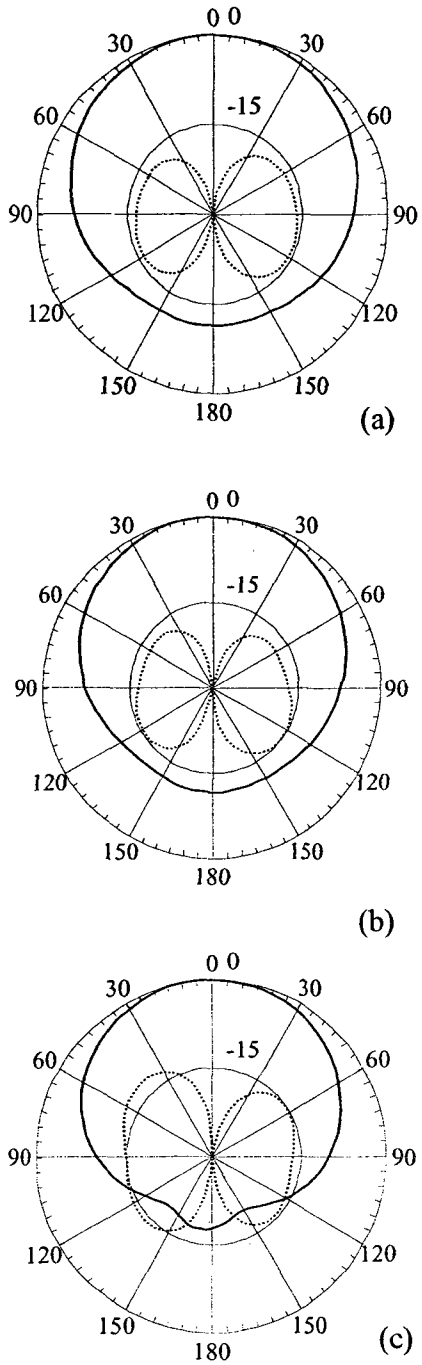

Figure 4.24: Co-polarized (solid), and cross-polarized (dash) fields in the H (y-z) plane, (a) f=5.2 GHz, (b) f=5.8 GHz, and (c) f=6.6 GHz.

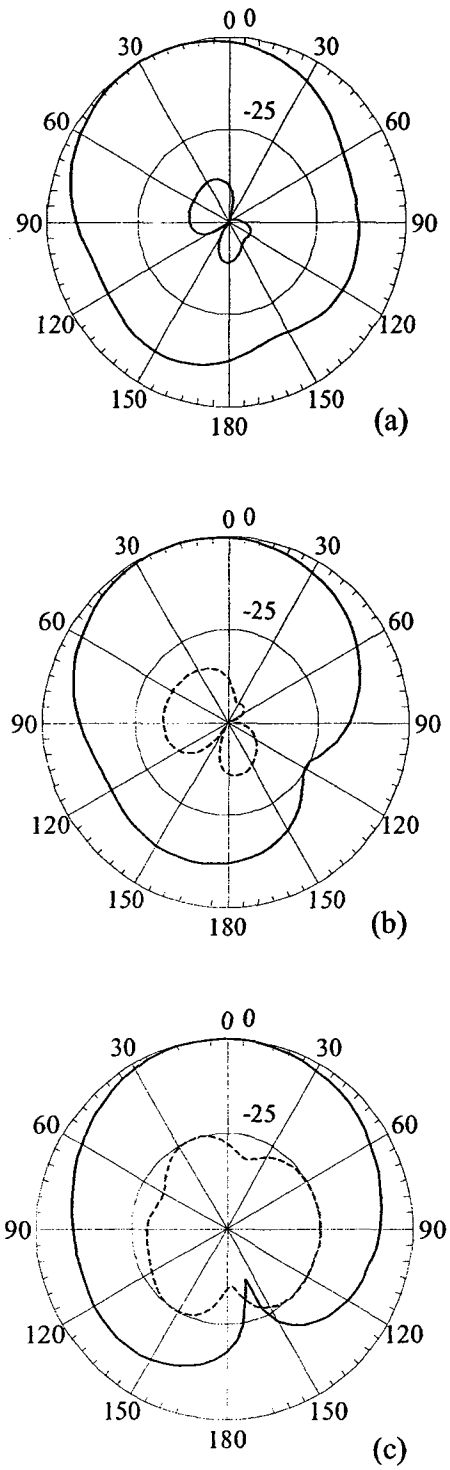

Figure 4.25: Co-polarized (solid), and cross-polarized (dash) fields in the E (x-z) plane, (a) f=5.2 GHz, (b) f=5.8 GHz, and (c) f=6.6 GHz.

The copolarized radiation patterns from HFSS and CST are plotted at a frequency value of 5.8 GHz for comparison. They are plotted in Figure 4.26.

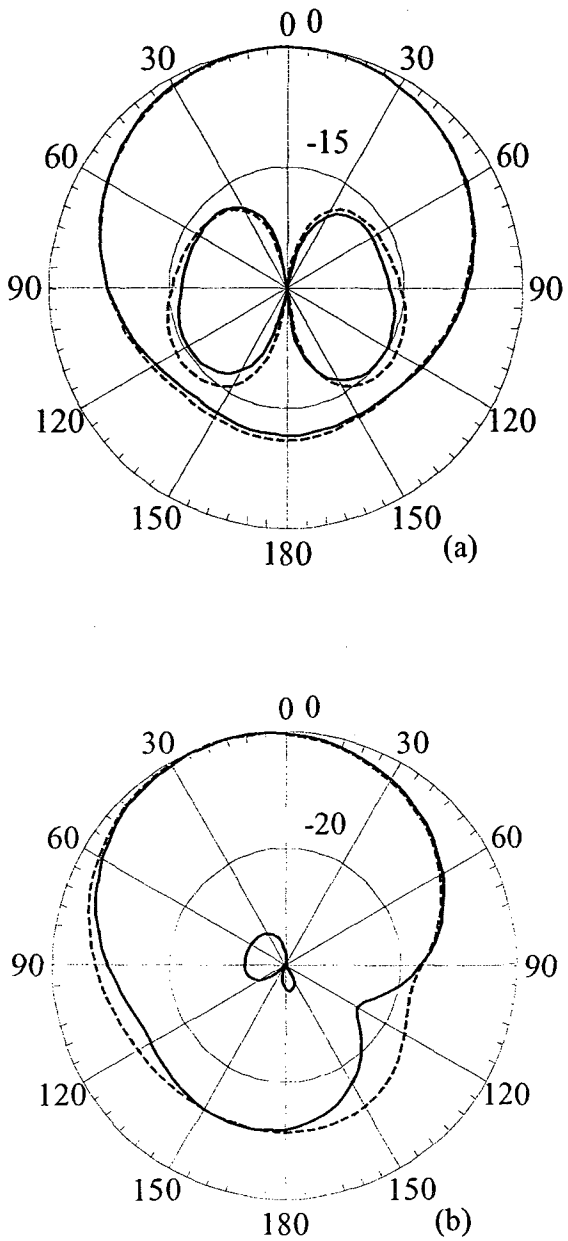

Figure 4.26 Co-polarized and cross polarized radiation patterns obtained from HFSS (solid) and CST (dash) in (a) H-plane, and (b) E-plane.

The measured radiation patterns in H and E planes are shown in figure 4.27. The measurement frequency is 5.8 GHz. The simulated radiation patterns are plotted on the same plot. As shown in the figure, there is a spillover of the radiation pattern which is a result of the electromagnetic scattering from the edges of the ground plane.

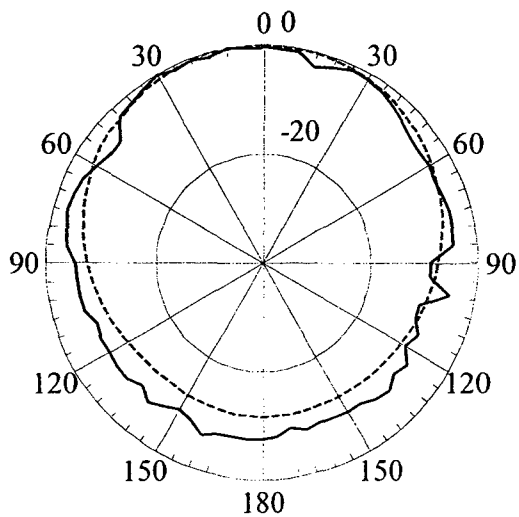

(a)

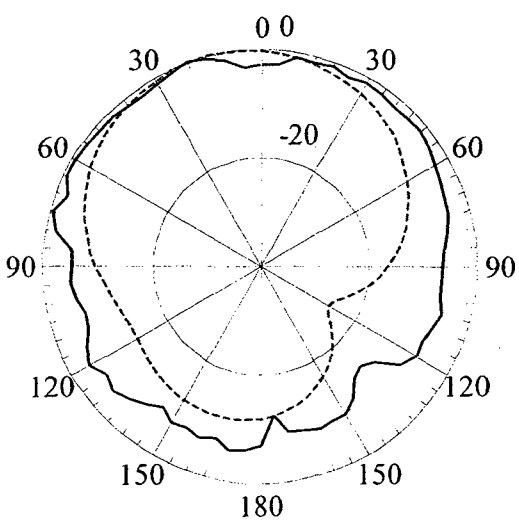

(b)

Figure 4.27: Measured (solid) and simulated (dash) radiation patterns in (a) H-plane, and (b) E-plane.

4.4 Compact DRA having an elliptical half cylinder geometry

In this section, a compact DRA with an elliptical half-cylinder shape is presented. Half-Elliptical DRAs haven't been proposed in the literature before and this thesis is presenting such kind of geometry. the DRA geometry is a half elliptical cylinder with a high major to minor radius ratio (R_1/R_2) to reduce the overall size of the antenna. The height of the half cylinder (h) is adjusted to be 15.5 mm. The antenna is fed by an aperture coupling slot. A parasitic U-shaped slot on the ground plane is used for more coupling and bandwidth enhancement. The antenna is mounted on a 30×20 mm^2 ground plane which is small enough for many applications. All geometrical parameters are shown in Figure 4.28. Although the size of the antenna is small, the antenna has good radiation characteristics and operates over a wide band of frequencies. Ansoft HFSS [64] and CST MWS are used for the antenna simulation. The antenna is fabricated and reasonable results are obtained. The Antenna impedance bandwidth is 32% for a return loss of S_{11} < -10dB. The proposed antenna has good radiation characteristics. As for the gain, it slightly changes over the antenna bandwidth[76].

The DR material is Rogers RO3010 ™ with ε_r=10.2, dielectric loss tangent of 0.0035. The substrate material is Rogers RT/Duroid 5880 ™ with ε_r=2.2, a loss tangent of 0.0009, and 0.767 mm thickness. The antenna is fed by a 50 Ω microstrip line

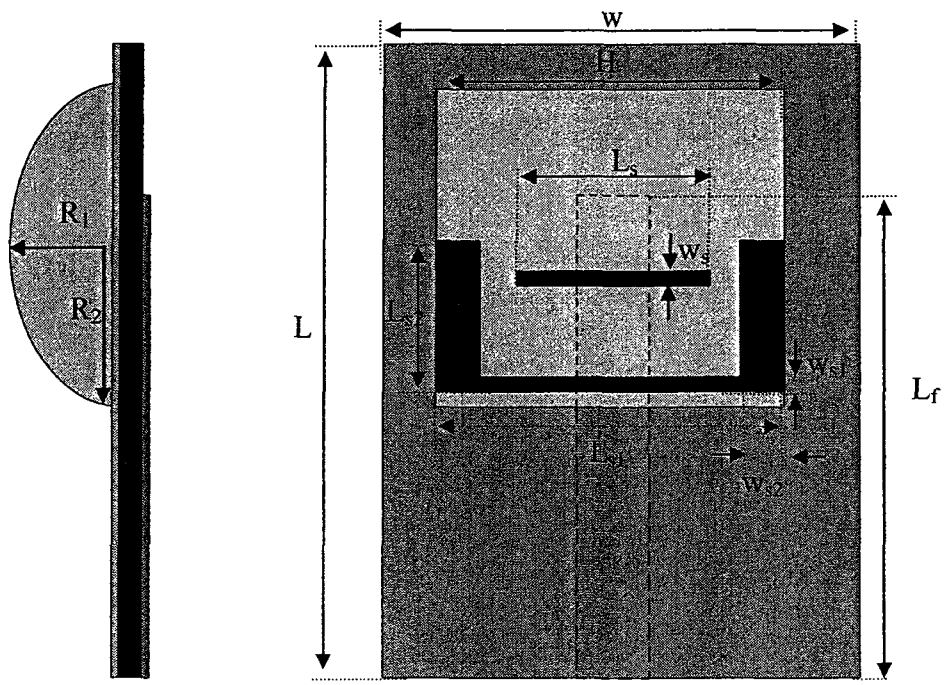

Figure 4.28 Geometry of the half volume elliptical DRA.

4.4.1 Design Verification

Ansoft HFSS is used to simulate the DRA and CST is used to verify the results obtained from HFSS. Both results obtained from both software packages are plotted in Figure 4.29. As shown in the figure, the antenna operates in the specified frequency range with a slight shift in the frequency because of the different techniques used for each tool.

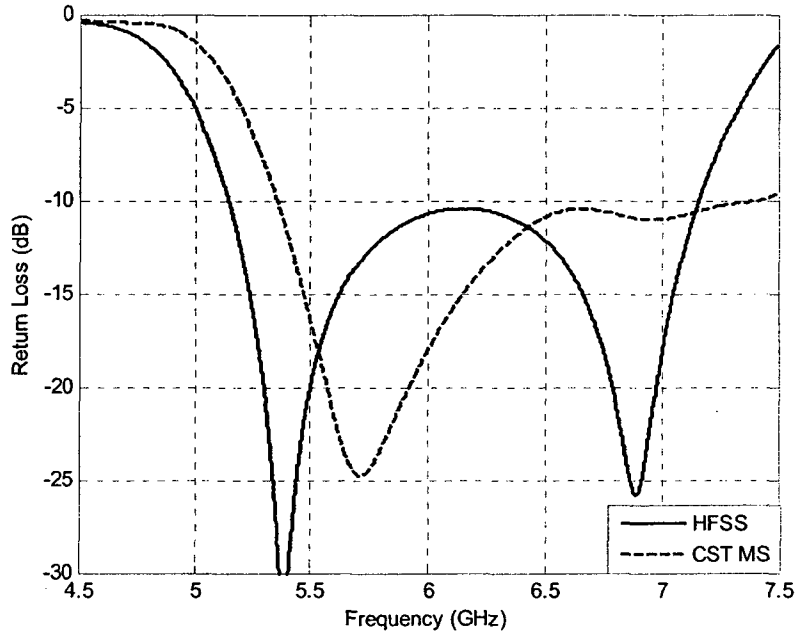

Figure 4.29 Return Loss obtained from HFSS and CST MS.

4.4.2 Effect of Ellipse minor to Major axis ratio (R_1/R_2)

Unlike the previous suggested antennas, the effect of the elliptical minor to major axis ratio is to be examined in this section because the other antenna elements are the same as those of the antennas presented earlier. In this case, the dielectric Resonator is made of a half elliptical cylinder to make it more compact. However, decreasing the minor to major axis ratio drastically changes the antenna resonance. Figure 4.30 shows the effect of the elliptical half cylinder minor to major axis. As it could be observed, the antenna will not resonate if the minor axis is too small.

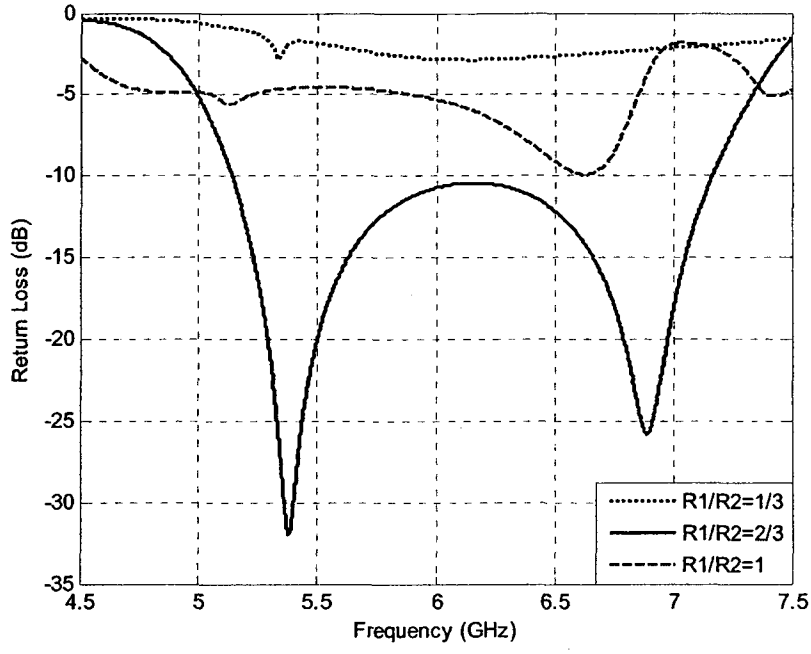

Figure: 4.30 Effect of minor to major axis ratio on the performance of the half volume elliptical DRA.

4.4.3 Impedance Bandwidth of the fabricated Compact DRA

After the parametric study has been done, the return loss of the optimized antenna is obtained by Ansof HFSS [64]. The DRA is fabricated and tested for the return loss. Figure 4.29 shows the fabricated half-cylindrical DRA and the antenna return loss is plotted with the simulated results in Figure 4.31. As it can be observed, a frequency shift occurs in the measured results which is because of the air gap between the DRA and the ground plane. The fabricated antenna operates from 5.4 GHz to 7.2 GHz.

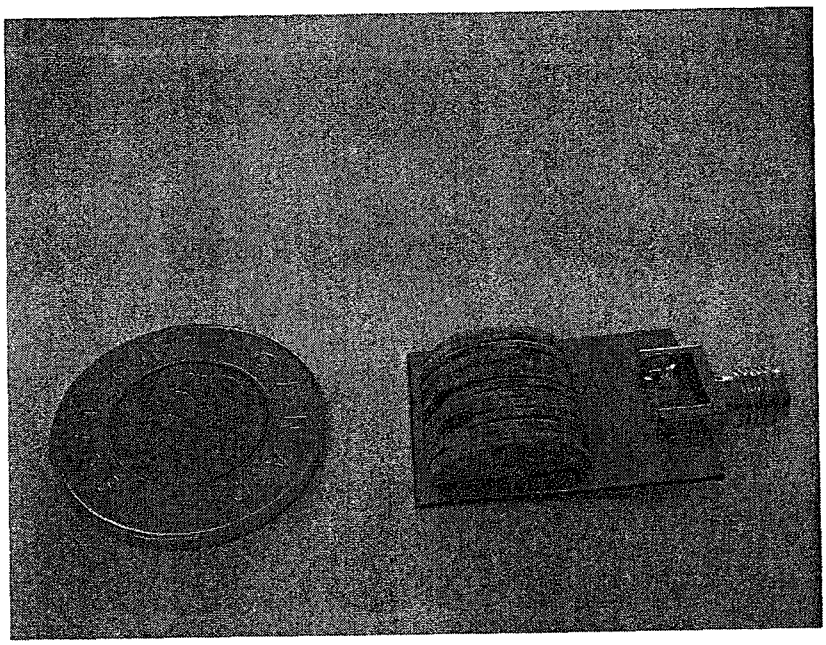

Figure: 4.31 A picture of the fabricated half elliptical DRA.

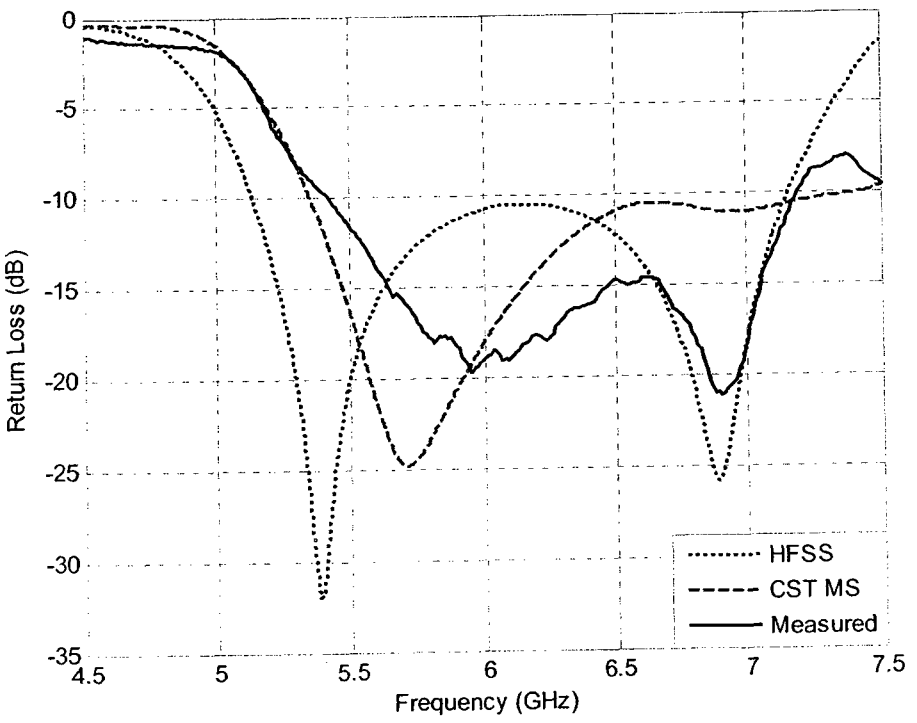

Figure: 4.32 Simulated and measured return loss of the half elliptical DRA.

4.4.4 Antenna Gain

The antenna gain in this model has more stable behavior than those obtained from the other two models. The antenna maintains a gain value of 5.5 dBi over the 5.6 - 6.6 GHz band. It has a value of 4 dBi at the edge frequencies. However, this slight change is acceptable in some applications. The antenna gain is shown in Figure 4.33.

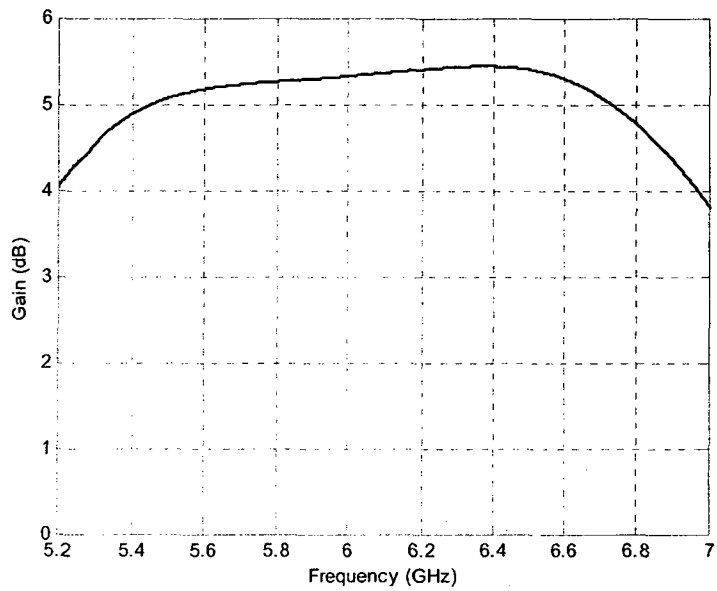

Figure: 4.33 Gain of the half elliptical DRA.

4.4.5 Antenna Radiation patterns

The antenna radiation patterns are computed in the E and H planes at three frequencies at different locations from the operating bandwidth. The antenna has the broadside characteristics with low cross-polarized levels in the H-plane. As for the E-plane, they are improved if they are compared to the results obtained from the other two

models. The cross-polarized fields level is also low in the E-plane. This can be shown in figures 4.34, and 4.35.

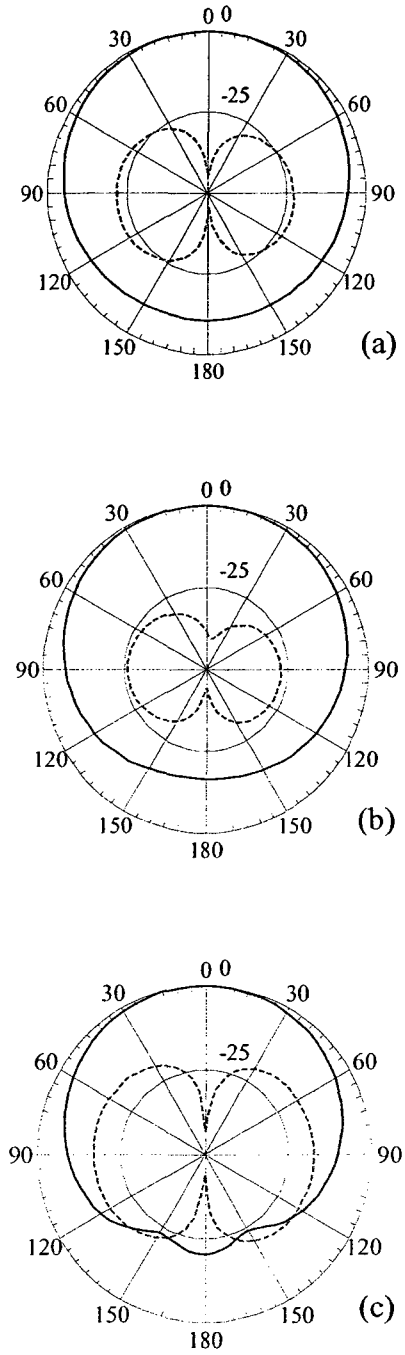

Figure 4.34: Co-polarized (solid), and cross-polarized (dash) fields in the H (y-z) plane, (a) f= 5.2 GHZ, (b) f=5.8 GHz, and (c) f=6.8 GHz.

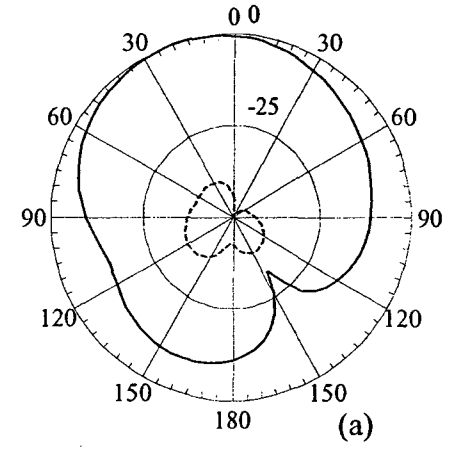

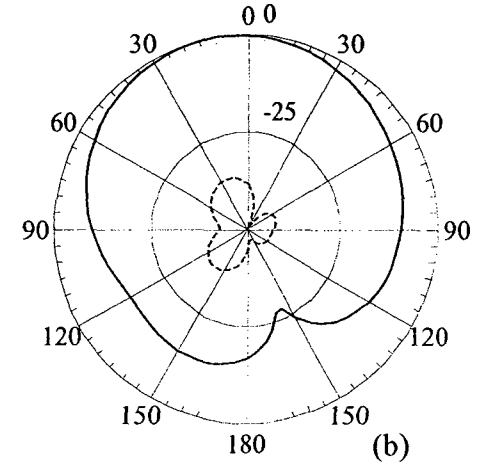

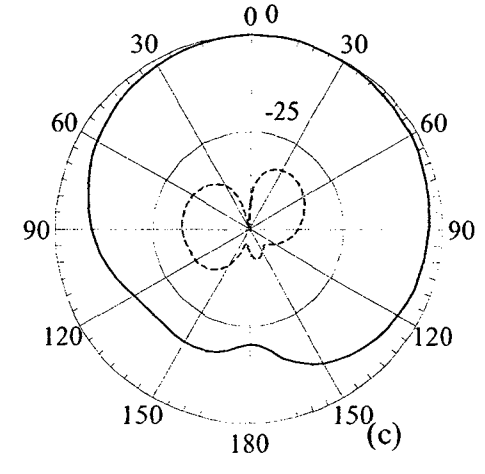

Figure 4.35: Co-polarized (solid), and cross-polarized (dash) fields in the E (x-z) plane, (a) f= 5.2 GHZ, (b) f=5.8 GHz, and (c) f=6.8 GHz.

The copolarized and the cross-polarized fields obtained from Ansoft HFSS and CST Microwave Studio are plotted in Figure 4.36. As it can be noticed that there is a good agreement between the radiation patterns obtained from both software packages.

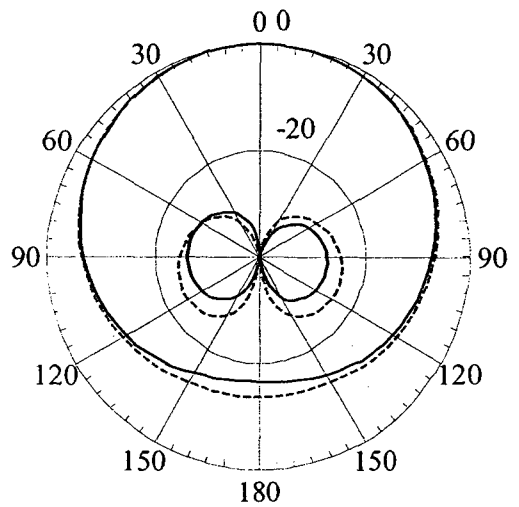

(a)

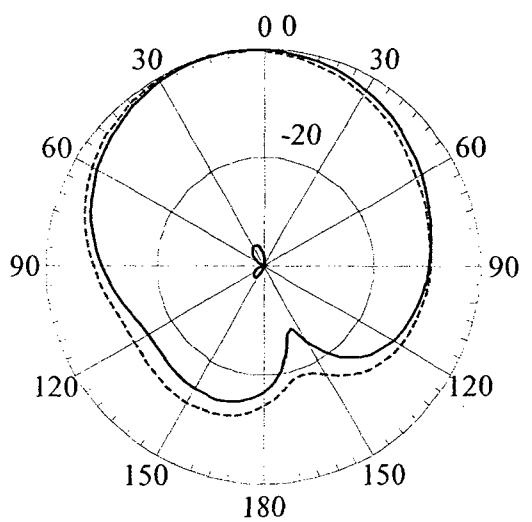

(b)

Figure 4.36 Co-polarized and cross polarized radiation patterns obtained from HFSS (solid) and CST (dash) in (a) H-plane, and (b) E-plane.

The measured radiation patterns in H and E planes are plotted together with the simulated ones as shown in Figure 4.37.

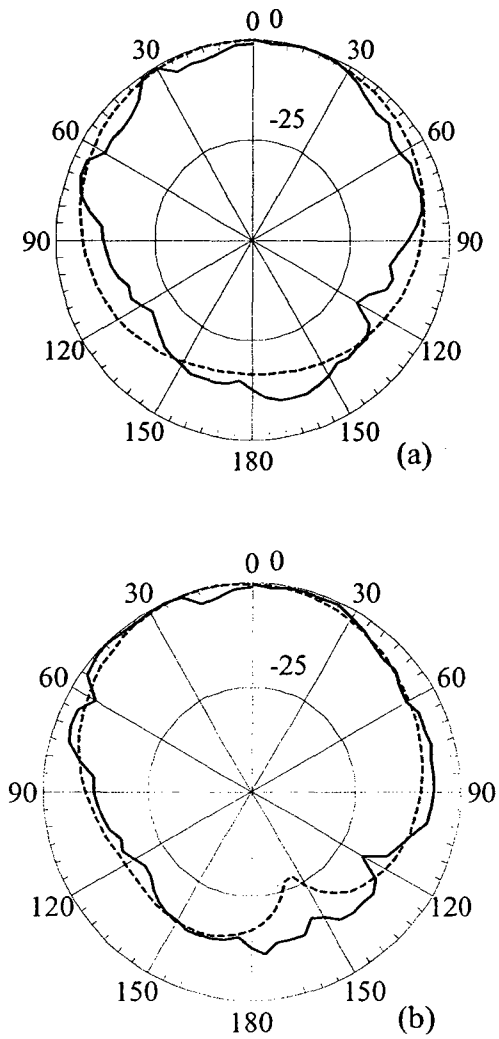

Figure 4.37Measured (solid) and simulated (dash) radiation patterns in (a) H-plane, and (b) E-plane.

The three antennas have broadband impedance characteristics, and broadside radiation patterns. The half volume EDRA is the best one because it is more compact in the z axis which can be embedded easily in the small equipment WLAN.

Chapter 5

Conclusions and Future Work

5.1 Highlights

The main goal of this research work is to study and design compact dielectric resonator antennas with broadband characteristics. A low permittivity dielectric material is used to improve the bandwidth of the DR Antenna because it has lower Q-factor. However, the size of the DRA is expected to be larger which is more challenging when designing a compact DRA. In this work, two different techniques are used to design a compact DRA. The half-cylindrical geometry and the parasitic U-shaped slot in the feeding network.

The half-cylindrical DRA is used to have the $TE_{01\delta}$ mode excited. Exciting this mode is useful because it radiates like a magnetic monopole which has the broadside radiation characteristics. Moreover, the rate of the $TE_{01\delta}$ resonant frequency change with respect to the cylindrical aspect ratio (a/h) is small which implies that the DRA excited at this mode have wide band characteristics. The half-cylindrical geometry is also used to minimize the size of the DRA. The elliptical half cylinder is also introduced to minimize the size of DRA in the z direction.

Another way introduced in this work to obtain broadband characteristics is the use of parasitic U-shaped slot surrounding the rectangular aperture feeding slot. The U-shaped

slot radiates like a magnetic dipole which has similar radiation characteristics to those of the DRA. The U shaped slot is designed to resonate at a lower frequency whereas the DRA is designed to resonate at the upper frequency to maintain a minimum size of the DRA at the higher frequency.

The parametric study is carried out using HFSS. The parametric study gives more understanding of the DRAs and a precise calculation of the antenna input impedance with the proposed feeding scheme. All the DRAs have been fabricated and tested for the impedance bandwidth as well as the radiation patterns.

The half cylindrical DRA models presented in this work offer good antenna characteristics as they proved a reasonable broadside radiation patterns in the E and H planes over the entire bandwidth. The gain slightly changes around 5 dBi which is good enough for the indoors wireless applications. A maximum bandwidth of 32% is obtained. By comparing the simulated and the measured DRAs results, there is a reasonable agreement between the simulated and the measured results as the frequencies are shifted in the measured impedance bandwidth because of the air gap between the DR and the ground plane.

5.2 Recommendations for Future Work

This thesis work focuses on the half-cyindrical DRAs being used for the broadband wireless applications. It can be expanded to ultrawideband wireless applications by

improving the impedance bandwidth. However, the radiation patterns should be tested at different frequencies over the entire band. The gain should be also tested.

For the experimental results, there is a frequency shift in the impedance bandwidth which is due to the air gap between the DRA and the ground plane. It is recommended to use dielectric powder between the DRA and the ground plane to compensate for this frequency shift.

For the radiation patterns, there is a spillover of the radiation because of the finite ground plane. This problem should be studied to improve the measured radiation patterns.

References

[1]. http://www.fcc.gov/pshs/techtopics/techtopics10, "License Except Wireless Applications for Public safety," technical topics, topic No.10, date of access: May25, 2009.

[2]. Leung, S.A., M.W. McAllister, and L.C. Shen, "The Resonant Cylindrical Dielectric Cavity Antenna," IEEE Transactions on Antennas & propagation, Vol.31, No.3, March 1983, pp. 406-412.

[3]. Binard, M.T., and R.V. Gelsthorpe, "Experimental Millimetric array Using Dielectric Radiators Fed by Means of Dielectric Waveguides," IEE Electronics Letters, Vol. 17, No. 18, Sept. 1981, pp. 633-635.

[4]. Haneishi, M., and H. Takazawa, "Broadband Circularly Polarized Planer Array Composed of a Pair of Dielectric Resonator Antennas," IEE Electronics Letters, Vol. 21, No. 18, May 1985, pp. 437-438.

[5]. A. Kishk, A. Glisson, and G. Junker, "Bandwidth enhancement for split cylindrical dielectric resonator antennas," Progress in Electromagnetics Research, PIER 33, pp.97-118, 2001.

[6]. Buerkle, A., K. Sarabandi, and H. Mosallaie, "Compact Slot and Dielectric Resonator Antenna with Dual-Resonance, Broadband Characteristics." IEEE Transactions Antennas & Propagation, Vol. 53, No. 3, March 2005, pp. 1020-1027.

[7]. Bijumon, P. V. et al., "Broadband Cylindrical Dielectric Resonator Antenna Excited by a modified Microstrip Line," IEE Electronics Letters, Vol. 41, No. 7, March 2005, pp. 385-387.

[8]. Menon, S. K., et al, "wideband cylindrical Dielectric Resonator Antenna Excited Using an L-Strip Feed," Microwave and Optical Technology Letters, Vol. 42, No. 4, Aug. 2004, pp. 293-294.

[9]. Li, B., and K.W. Leung, "Strip-Fed Rectangular Dielectric Resonator Antenna with/without a Parasitic Patch," IEEE Transactions on Antennas & Propagation, Vol. 53No. 7, July 2005, pp. 2200-2207.

[10]. Simons, R.N., and R.Q. Lee, "Effect of Parasitic Dielectric Resonator on CPW/Aperture-Coupled Dielectric Resonator Antennas," IEE Proceedings Part-H, Vol. 140, No.5, Oct. 1993, pp. 336-338.

[11]. Alsharkawy, M., A.Z. Elsherbeni, and C.E. Smith, "stacked Elliptical Dielectric Resonator Antennas for Wideband Applications," IEEE Antenna & Propagation Symposium Digest 2004, Monterey, CA, Vol. 2, pp. 1371-1374.

[12]. Fan, Z., et al., " Parasitic Coplanar Three-Element Dielectric Resonator AntennaSubarry," IEE Electronics Letters, Vol. 32, No. 9, April 1996, pp. 789-790.

[13]. Kishk, A.A., B. Ahn, and D. Kajfez, "Broadband Stacked Dielectric-Resonator Antennas," IEE Electronics Letters, Vol. 25, No. 18, Aug. 1989, pp. 1232-1233.

[14]. Kishk, A.A., et al., "Numerical Analysis of Stacked Dielectric Resonator Antennas Excited by a Coaxial Probe," IEEE transactions on Antennas & Propagation, Vol.51, No. 8, Aug. 2003, pp. 1996-2005.

[15]. Leung, K.W., et al., "Bandwidth Enhancement of Dielectric Resonator Antenna by Loading a Low-Profile Dielectric Disk of Very High Permittivity," IEE Electronics Letters, Vol. 33, No. 9, April 1997, pp. 725-726.

[16]. A. A. Kishk, "Dielectric Resonator Antenna, A candidate for Radar applications,"IEEE Radar Conference, 2003, p.p 258-264.

[17]. Rao, Q., T.A. Denidni, and A.R. Sebak, "Experimental Results of a Low Profile Broadband Dielectric Resonator Antenna," IEEE Antennas & Propagation Letters, No. 54, 2005.

[18]. Lappierre, M., et al., "Ultra Wideband Monopole/Dielectric Resonator Antenna," IEEE Microwave and Wireless Components Letters, Vol. 15, No. 1, Jan. 2005, pp. 7-9.

[19]. HFSS, v10, Ansoft Corporation Software, Pittsburgh, PA, USA. 2006.

[20]. CST MICROWAVE STUDIO, 2006B.

[21]. J. Van Bladel, "On the resonances of a dielectric resonator of very high permittivity," IEEE Trans. Microwave Theory Tech., vol. MTT-23, Feb. 1975, pp. 199–208.

[22]. A. Karp, H. J. Shaw, and D. K. Winslow, "Circuit properties of microwave dielectric resonator," IEEE Trans. Microwave Theory Tech., vol. MTT-16, Oct. 1968, pp. 810–828.

[23]. R. K. Mongia, "Theoretical and experimental resonant frequencies of rectangular dielectric resonators," Proc. Inst. Elect. Eng., vol. 139, pt. H, Feb. 1992, pp. 98–104.

[24]. Gastine, M., L. Courtois, and J. J. Dormann, "Electromagnetic Resonances of Free Dielectric Spheres," IEEE Transactions on Microwave Theory & Techniques, Vol. 15, No. 12, Dec. 1967, pp. 694-700.

[25]. Kishk, A. A., G. Zhou, and A. W. Glisson, " Analysis of Dielectric Resonator Antennas with Emphasis on Hemispherical Structures," IEEE Electronics Letters, Vol. 20, No. 2, April 1994, pp. 20-31.

[26]. Verplanken, M., and J. Van Bladel, "The magnetic –Dipole Resonance of Ring Resonators of Very High permittivity," IEEE Transactions on Microwave Theory& Techniques, Vol. 27, No. 4, April 1979, pp. 328-332.

[27]. Luk, K. M., and Leung, K. W., "Dielectric Resonator Antennas," Baldock, Hertfordshire, England: Research Studies Press Ltd., 2003.

[28]. Petosa, A., " Dielectric Resonator Antenna Handbook," Boston/London: Artech House, 2007.

[29]. Verplanken, M., and J. Van Bladel, "The magnetic –Dipole Resonance of Ring Resonators of Very High permittivity," IEEE Transactions on Microwave Theory& Techniques, Vol. 27, No. 4, April 1979, pp. 328-332.

[30]. G. P. Junker, A. A. Kishk and A. W. Glisson, "Input impedance of dielectric resonator antennas excited by a coaxial probe," IEEE Trans. Antennas Propagat., vol. 42, July 1994, pp. 960-966.

[31]. S. M. Shum and K. M. Luk, "FDTD analysis of probe-fed cylindrical dielectric resonator antenna," IEEE Trans. Antennas Propagat., vol. 46, Mar. 1998, pp. 325-333.

[32]. A. Ittipiboon, R. K. Mongia, Y. M. M. Antar, P. Bhartia and M. Cuhaci, "Aperture-fed rectangular and triangular dielectric resonators for use as magnetic dipole antennas," Electron. Lett., vol. 29, Nov. 1993, pp. 2001-2002.

[33]. K. W. Leung, K. M. Luk and E. K. N Yung, "Spherical cap dielectric resonator antenna using aperture coupling," Electron. Lett., vol. 30, No. 17, Aug. 1994, pp. 1366-1367.

[34]. J. T. H. St. Martin, Y. M. M. Antar, A. A. Kishk and A. Ittipiboon, "Dielectric resonator antenna using aperture coupling," Electron. Lett., vol. 26, Nov. 1990, pp. 2015-2016.

[35]. G. P. Junker, A. A. Kishk and A. W. Glisson, "Input impedance of aperture-coupled dielectric resonator antennas", IEEE Trans. Antennas and Propagat., vol. 44, May 1996, pp. 600-607.

[36]. K. W. Leung, W. C. Wong, K. M. Luk, and E. K. N. Yung, "Annular slot-coupled dielectric resonator antenna," Electron. Lett., vol. 34, No. 13, June 1998, pp. 1275-1277.

[37]. K. W. Leung, "Analysis of aperture-coupled hemispherical dielectric resonator antenna with a perpendicular feed," IEEE Trans. Antennas Propagat., vol. 48, No. 6, June 2000, pp. 1005-1007.

[38]. K. Y. Chow and K. W. Leung, "Theory and experiment of the cavity-backed slot-excited dielectric resonator antenna," IEEE Trans. Electromagnetic Compatibility, vol. 42, No. 3, Aug. 2000, pp. 290-297.

[39]. K. Y. Chow, K. W. Leung, K. M. Luk and E. K. N. Yung, "Input impedance of the slot-fed dielectric resonator antenna with/without a backing cavity," IEEE Trans. Antennas Propagat., vol. 49, Feb. 2001, No. 2, pp. 307-309.

[40]. R. A. Kranenburg and S. A. Long, "Microstrip transmission line excitation of dielectric resonator antennas", Electron. Lett., vol. 24, Sept. 1988, pp. 1156-1157.

[41]. K. W. Leung, K. Y. Chow, K. M. Luk and E. K. N. Yung, "Low-profile circular disk DR antenna of very high permittivity excited by a microstrip line," Electron. Lett., vol. 33, No. 12, June 1997, pp. 1004-1005.

[42]. R. A. Kranenburg, S. A. Long and J. T. Williams, "Coplanar waveguide excitation of dielectric resonator antennas", IEEE Trans. Antennas Propagat. vol. 39, Jan. 1991,pp. 119-122.

[43]. Gastine, M., L. Courtois, and J. J. Dormann, "Electromagnetic Resonances of Free Dielectric Spheres," IEEE Transactions on Microwave Theory & Techniques, Vol. 15, No. 12, Dec. 1967, pp. 694-700.

[44]. Kranenburg, R. A., and S. A. Long, "Microstrip Transmission Line Excitation of Dielectric Resonator Antennas," IEE Electronics Letters, Vol. 24, No. 18, Sept. 1988, pp. 1156-1157.

[45]. Al Salameh, M. S.., Y.M.M. Antar, and G. Seguin, "Coplanar-Waveguide –Fed Slot-Coupled Rectangular Dielectric Resonator Antenna," IEEE Transactions on Antennas & Propagation, Vol. 50, No. 10, Oct. 2002, pp. 1415-1419.

[46]. Deng, S.M., et al., "CPW-Fed Ceramic Dielectric Resonator Antenna with High Profile," IEEE Antennas & Propagation Symposium Digest AP-S 2004, Monterey CA, Vol. 1, pp. 1098-1101.

[47]. Deng, S.M., et al., "CPW-Fed Dual Rectangular Ceramic Dielectric Resonator Antenna Through Inductively Coupled Slots," IEEE Antennas & Propagation Symposium Digest AP-S 2004, Monterey CA, Vol. 1, pp. 1102-1105.

[48]. Mongia, R.K., et al., " A Half-Split Cylindrical Dielectric Resonator Antenna Using Slot Coupling," Microwave and guided Wave Letters, Vol.3, No.2, Feb. 1993, pp.38-39.

[49]. Leung, K.W., et al., "Input Impedance of Aperture Coupled Hemispherical Dielectric Resonator Antenna," IEE Electronics Letters, Vol. 29, No. 13, March 1993, pp. 1165-1167.

[50]. Leung, K.W., et al., "Theory and Experiment of an Aperture-Coupled Hemispherical Dielectric Resonator Antenna," IEEE Transactions on Antennas & Propagation, Vol. 43, No. 1, Nov. 1995, pp. 1192-1198.

[51]. Leung, K.W., et al., "Annular-Slot-Coupled Dielectric Resonator Antenna," IEE Electronics Letters, Vol.34,No. 13, June 1998, pp.1275-1277.

[52]. A. Ittipiboon, R. K. Mongia, Y. M. M. Antar, P. Bhartia and M. Cuhaci, "Aperture-fed rectangular and triangular dielectric resonators for use as magnetic dipole antennas," Electron. Lett., vol. 29, Nov. 1993, pp. 2001-2002.

[53]. Huang, C.Y., Wu, and K.L. Wong, "Cross-Slot-Coupled Microstrip Antenna and Dielectric Resonator Antenna for Circular Polarization," IEEE Transactions on Antennas & Propagation, Vol. 47, No. 4, April 1999, pp. 605-609.

[54]. Huang, C.Y., and C.F. yang, " Cross-Aperture Coupled Circularly-polarized Dielectric Resonator Antenna," IEEE Antennas and Propagation Symposium Digest AP-S 1999, Orlando, FL, pp. 34-37.

[55]. G. P. Junker, A. A. Kishk and A. W. Glisson, "Input impedance of aperture-coupled dielectric resonator antennas", IEEE Trans. Antennas and Propagat., vol. 44, May 1996, pp. 600-607.

[56]. Kishk, A.A., "Experimental Study of Broadband Embedded Dielectric Resonator Antennas Excited by a Narrow Slot," Antennas and Wireless Propagation Letters, Vol. 4, 2005, pp. 79-81.

[57]. Sangiovanni, A., J.Y. Dauvignac, and C. Pichot, "Embedded Dielectric Resonator Antenna for Bandwidth Enhancement," IEE Electronics Letters, Vol. 33, No. 25, Dec. 1997, pp. 2090-2091.

[58]. Kishk, A.A., A.W. Glisson, and Y. Yin, "Conical Dielectric Resonator Antennas Excited by a Coaxial Probe," Microwave Optical Technology Letters, Vol. 29, No. 3, May 2001, pp. 160-162.

[59]. Chair, R., et al., "Wideband Flipped Staired Pyramid Dielectric Resonator Antennas," IEE Electronics Letters, Vol.2, pp. 1375-1378.

[60]. Chair, R., et al., "Broadband Aperture-Coupled Flipped Staired Pyramidal and Conical Dielectric Resonator Antennas," IEEE Antennas & Propagation Symposium Digest AP-S 2004, Monterey, CA, Vol. 2, pp. 1375-1378.

[61]. Pliakostathis, K., and D. Mirshekar-Syahkal, "stepped Dielectric Resonator Antennas for wideband Applications," IEEE Antennas & Propagation Symposium Digest, APS-2004, Monterey, CA, Vol. 2, pp. 1367-1370.

[62]. Ittipiboon, A., et al., "Broadband Nonhomogeneous Multisegment Dielectric Resonator Antenna," US patent 5,952,972, Sept. 14, 1999.

[63]. Ittipiboon, A., et al., "An Investigation of a Novel Broadband Dielectric Resonator Antenna," IEEE Antennas & Propagation Symposium Digest APS-1996, Baltimore, MD, pp. 2038-2041.

[64]. Rao, Q., T.A. Denidni, and A.R. Sebak, "Experimental Results of a Low Profile Broadband Dielectric Resonator Antenna," IEEE Antennas & Propagation Letters, No. 54, 2005.

[65]. Lappierre, M., et al., "Ultra Wideband Monopole/Dielectric Resonator Antenna," IEEE Microwave and Wireless Components Letters, Vol. 15, No. 1, Jan. 2005, pp. 7-9.

[66]. C. A. Balanis, "Advanced Engineering Electromagnetics," John Wiley and Sons, 1989.

[67]. J. Jin, "The Finite Element Method in Electromagnetics," John wiley and Sons, 1993.

[68]. Shum, S.M., and K.M. Luk, "FDTD Analysis of Probe-Fed Cylindrical Dielectric Resonator Antenna," IEEE transactions on Antennas & Propagation, Vol. 46, No.3, March 1998, pp. 325-333.

[69]. Douib, A., et al., "TLM Analysis of Rectangular dielectric Resonator antennas," IEEE Antennas & Propagation symposium Digest AP-S1995, Newport Bech, CA, pp. 782-785.

[70]. I. Munteanu, F. Hirtenfelder, "Convergence of the Finite Integration Technique on Various Mesh Types," German Microwave Conference GeMiC, 2005, pp. 209-212.

[71]. Glisson, A.W., D. Kajfez, and J. James, "Evaluation of Modes in Dielectric Resonators using a surface integral Equation Formulation," IEEE Transactions on Microwave Theory& Techniques, Vol.31, Dec. 1983, pp. 1023-1029.

[72]. D. Pozar, "Microwave Engineering," 3rd edition, Wiley and Sons, New York, 2005.

[73]. Abumazwed, A., O. Ahmed, and A. R. Sebak, "Broadband half-cylindrical DRA for Future WLAN Applications," 3rd European Conference on Antennas & Propagation, Eucap, 23-27 March 2009, pp. 389-392.

[74]. Kouyoumjian, R.G., and P.H. Pathak, "A Uniform Geometric Theory of Difraction for an Edge in a Perfectly Conducting Surface," Proceedings of the IEEE, Vol. 62, Nov. 1974, pp.1448-1461.

[75]. Abumazwed, A., and A. R. Sebak, "Compact DRA for Broadband Applications," IEEE International Symposium on Antennas & Propagation AP-S/URSI, South Carolina, June 2009.

[76]. Abumazwed, A., and A. R. Sebak, "Compact Dielectric Resonator Antenna for Broadband Applications (5.2/5.8GHz)," 3rd European Conference on Antennas & Propagation, Eucap, 23-27 March 2009, pp. 433-436.